Supporting Information for

Terminal vs Bridging Hydrides of Diiron Dithiolates: Protonation of $Fe_2(dithiolate)(CO)_2(PMe_3)_4$

Riccardo Zaffaroni, Thomas B. Rauchfuss*, Danielle L. Gray
Luca De Gioia and Giuseppe Zampella*

Contents

Figure S1. ^{1}H NMR spectrum of a CD_2Cl_2 solution of $Fe_2(edt)(CO)_2(PMe_3)_4$ at -90 °C.

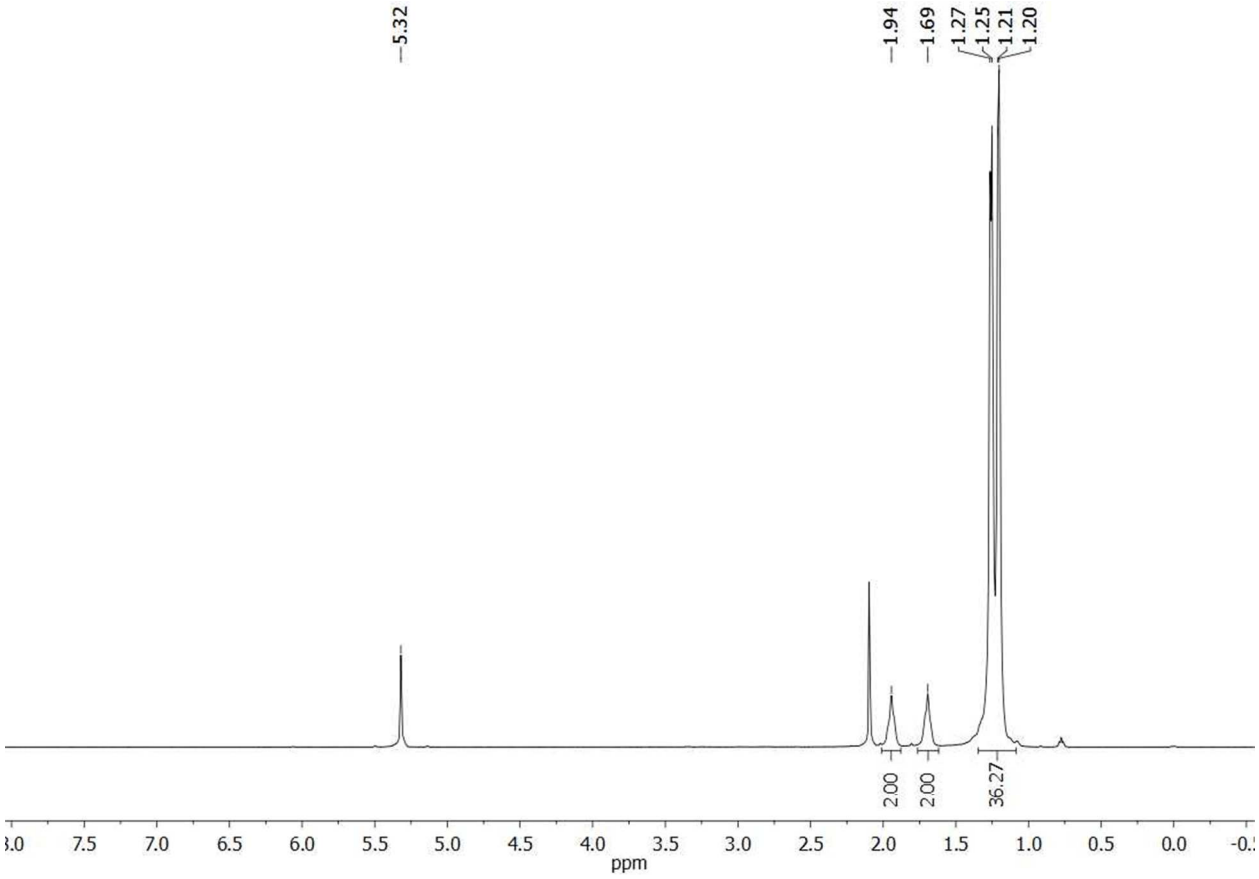

Figure S2. $^{31}P\{^{1}H\}$ NMR spectrum of a CD_2Cl_2 solution of $Fe_2(edt)(CO)_2(PMe_3)_4$ at -90 °C.

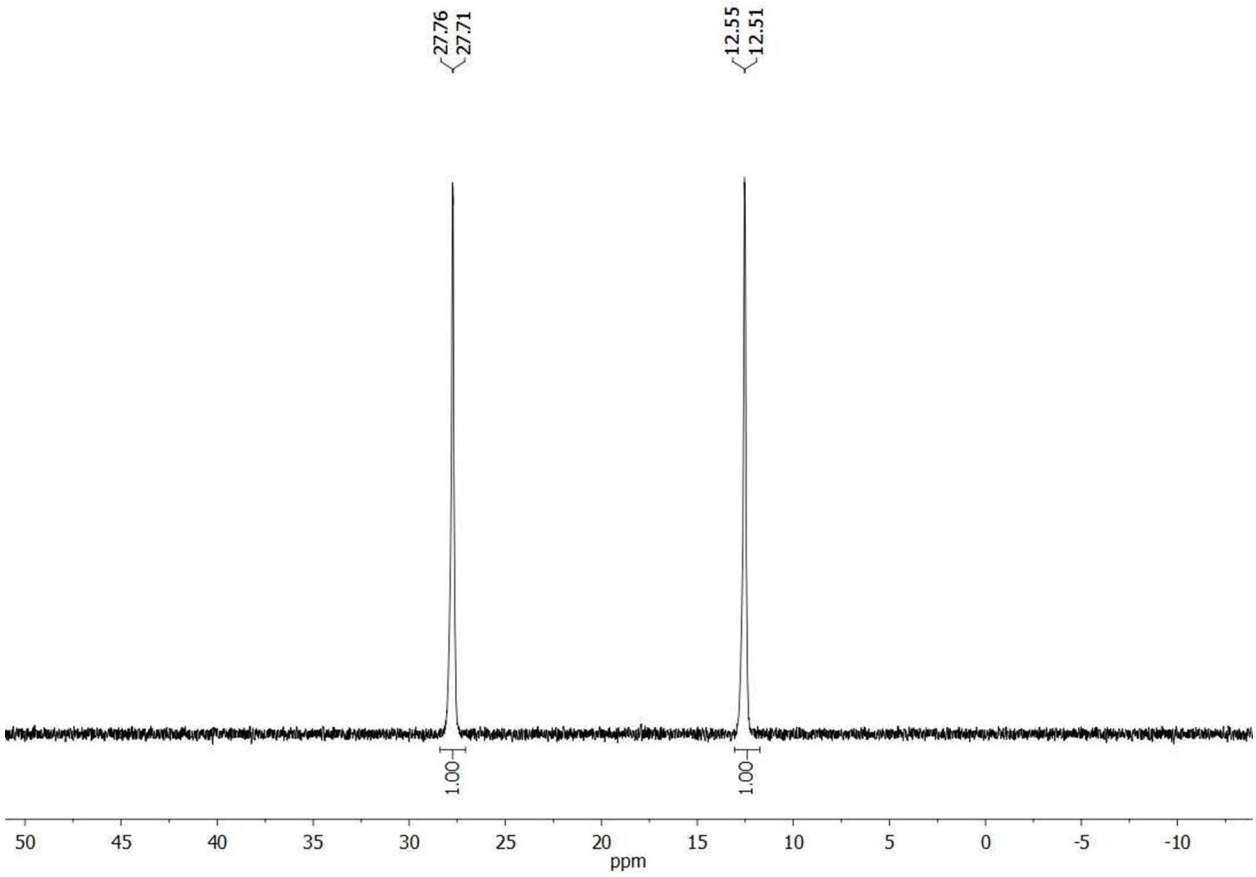

Figure S3. ^{1}H NMR spectrum for protonation of $Fe_2(edt)(CO)_2(PMe_3)_4$ with one equiv of $H(OEt_2)_2BAr^F{}_4$ at -90 °C in CD_2Cl_2 solution.

Procedure: 5 mg of compound **1** were weighted inside a J. Young tube and dissolved in minimal amount (0.3 mL) of CD_2Cl_2. This solution was frozen at liquid nitrogen temperature and the tube evquated before 0.2 mL of CD_2Cl_2 were distilled on top of the first frozen solution. A 0.2 mL solution of 8.9 mg of $H(OEt_2)_2BAr^F{}_4$ was injected in the tube. The solution was allowed to thaw at -90 °C for 15 min before the tube was vigorously shaken and inserted into the precooled NMR probe.

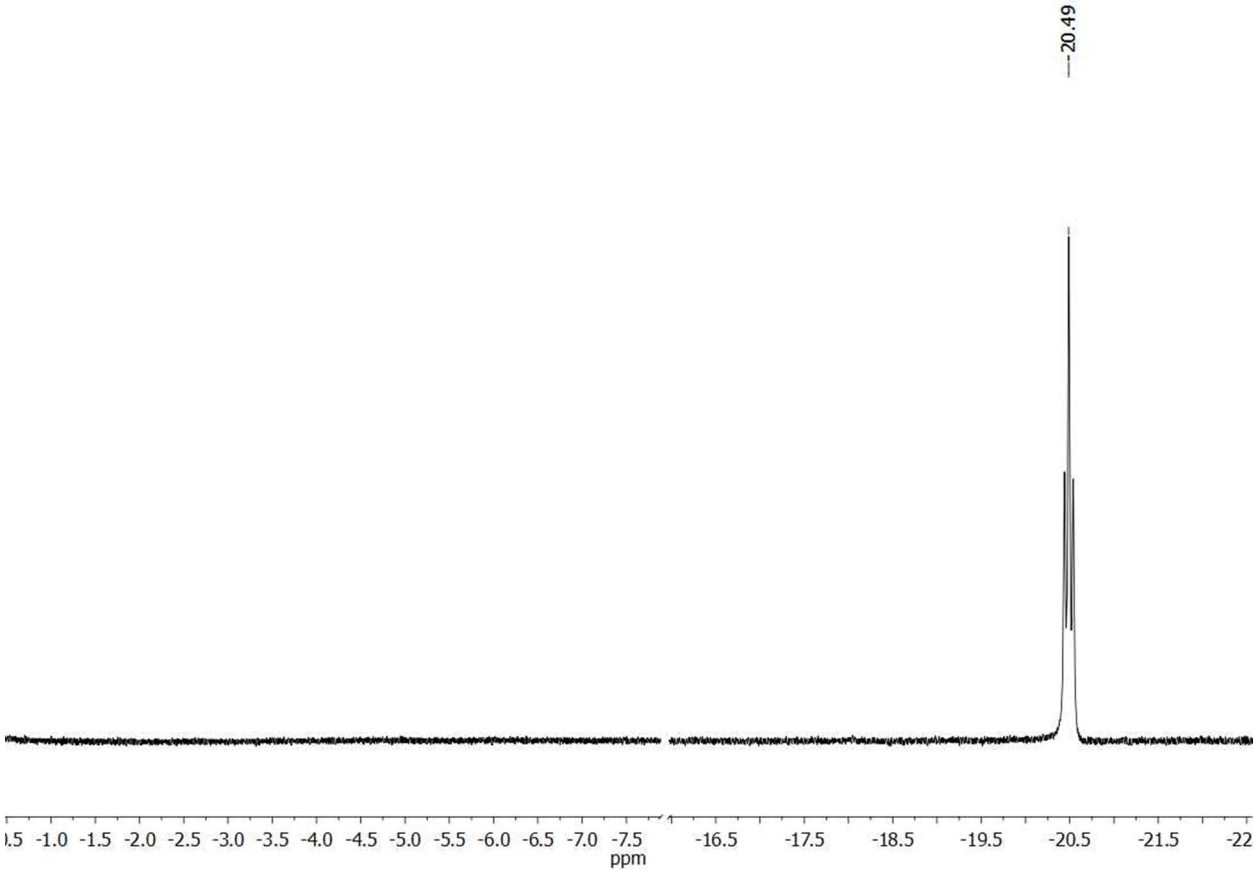

Figure S4. Cyclic voltammogram of $Fe_2(edt)(CO)_2(PMe_3)_4$ in 1,2-difluorobenzene referenced to Fc/Fc^+.

Conditions and Results: Complex = 1 mM; $[TBA]PF_6$ = 100 mM. $E_{½}$ = -950 mV (i_{pa}/i_{pc} = 0.92).

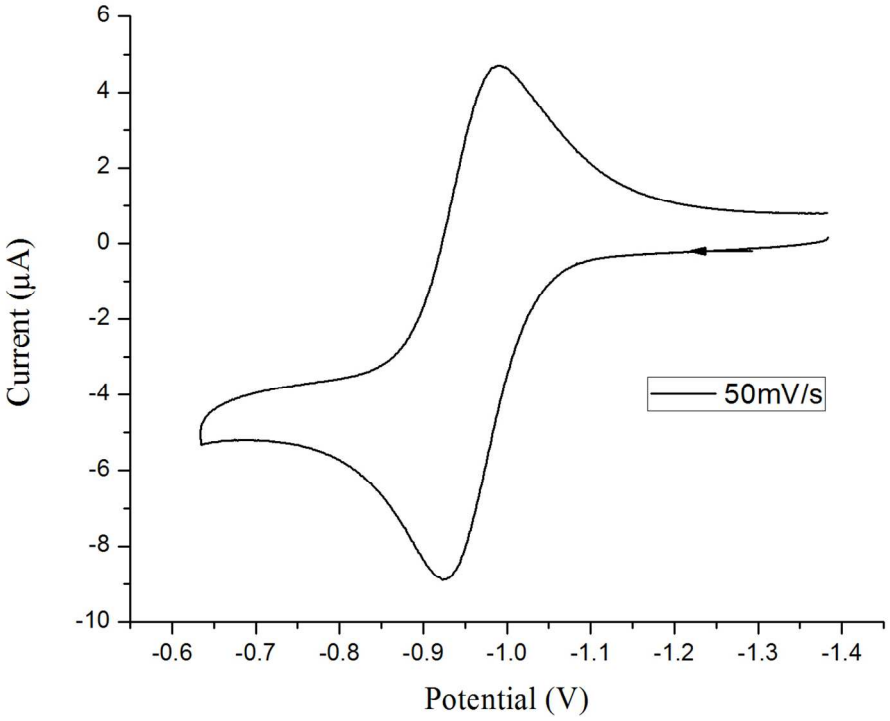

Figure S5. ^{1}H NMR spectrum for protonation of $Fe_2(edt)(CO)_2(PMe_3)_4$ with one equiv of $H(OEt_2)_2BAr^F{}_4$ at room temperature in CD_2Cl_2 solution.

Procedure: 5 mg of $Fe_2(edt)(CO)_2(PMe_3)_4$ and 8.9 mg of $H(OEt_2)_2BAr^F{}_4$ were weighted into a J. Young tube then dissolved in 0.7 mL of CD_2Cl_2 at room temperature. The tube was immediately inserted into the NMR probe at +20 °C.

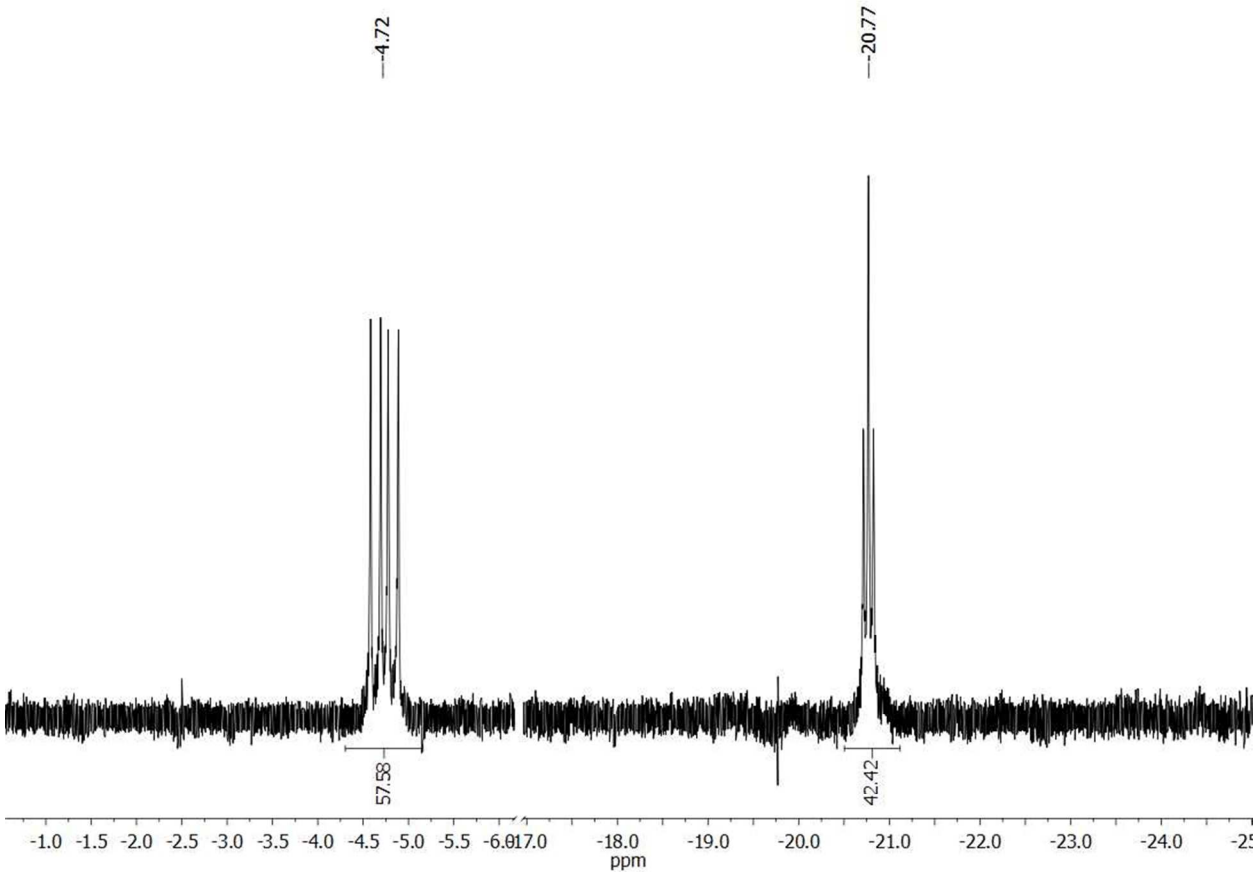

Figure S6. ^{31}P $\{^{1}H\}$ NMR spectrum of a CD_2Cl_2 solution of $Fe_2(pdt)(CO)_2(PMe_3)_4$ at -90 (bottom), -70 (middle), 0 °C (top).

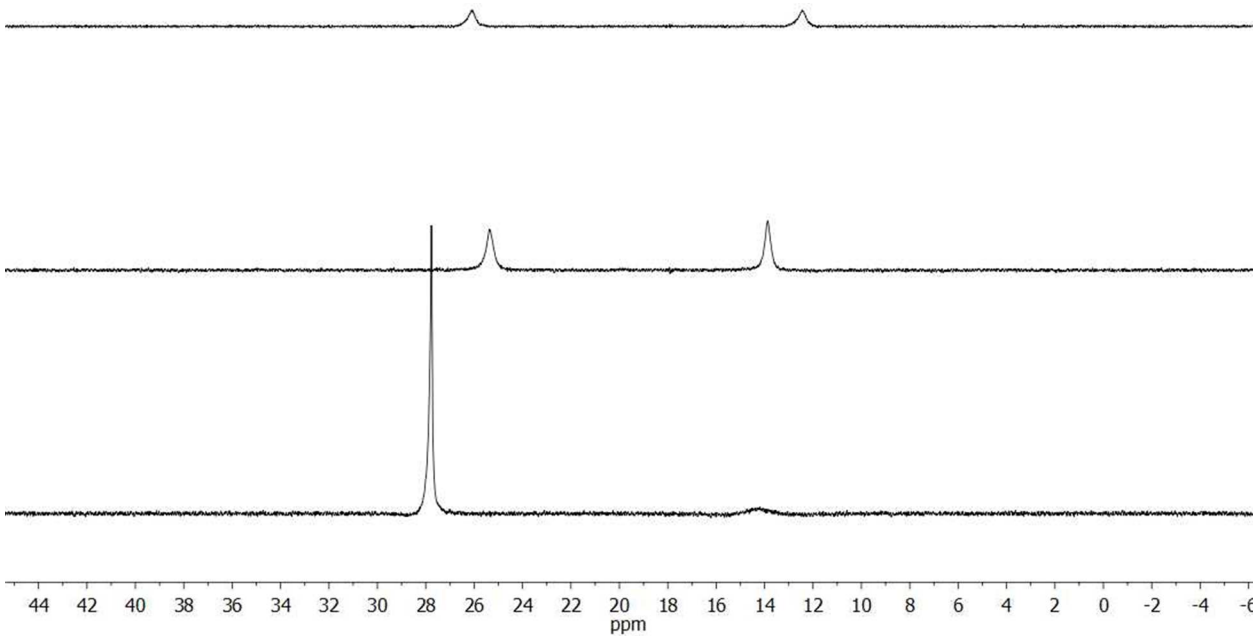

Figure S7. Cyclic voltammogram of $Fe_2(pdt)(CO)_2(PMe_3)_4$ in 1,2-difluorobenzene referenced to Fc/Fc^+.

Conditions and Results: Complex = 1 mM; $[TBA]PF_6$ = 100 mM. $E_{½}$ = -970 mV (i_{pa}/i_{pc} = 0.80).

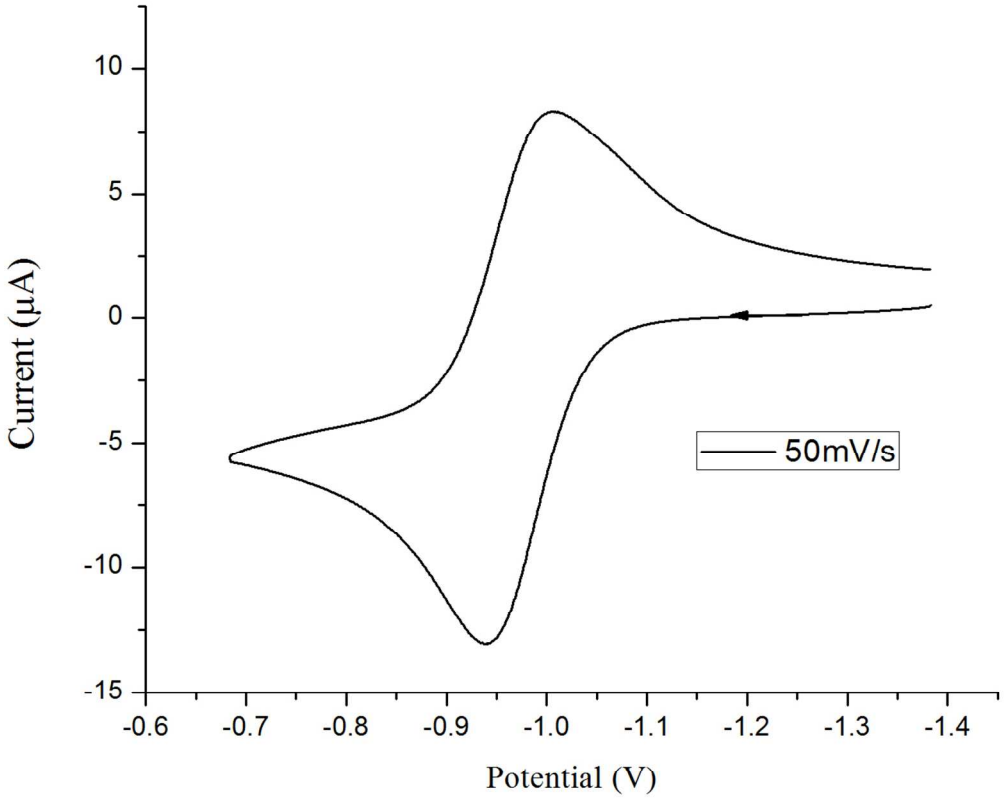

Figure S8. $^{31}P\{^{1}H\}$ NMR spectrum for protonation of $Fe_2(pdt)(CO)_2(PMe_3)_4$ with one equiv of $H(OEt_2)_2BAr^F{}_4$ at -90 °C in CD_2Cl_2 solution. Three species are present in solution, [μ-H**2**]$^+$, [*t*-H**2**]$^+$ and the S-protonated species [*S*-H**2**]$^+$ in a 2:1:1 ratio.

Assignments: The four singlets at δ 30.02, 27.79, 14.51 and 11.62 are assigned to the S-protonated species [*S*-H**2**]$^+$. The doublets centered at δ 25.8 and 20.are assigned to the hydride [μ-H**2**]$^+$. Signals centered at δ 36.59, 31.0, and 18.83 are assigned to the terminal hydride [*t*-H**2**]$^+$, a fourth signal is present but obscured by the [μ-H**2**]$^+$ signal at δ 25.8.

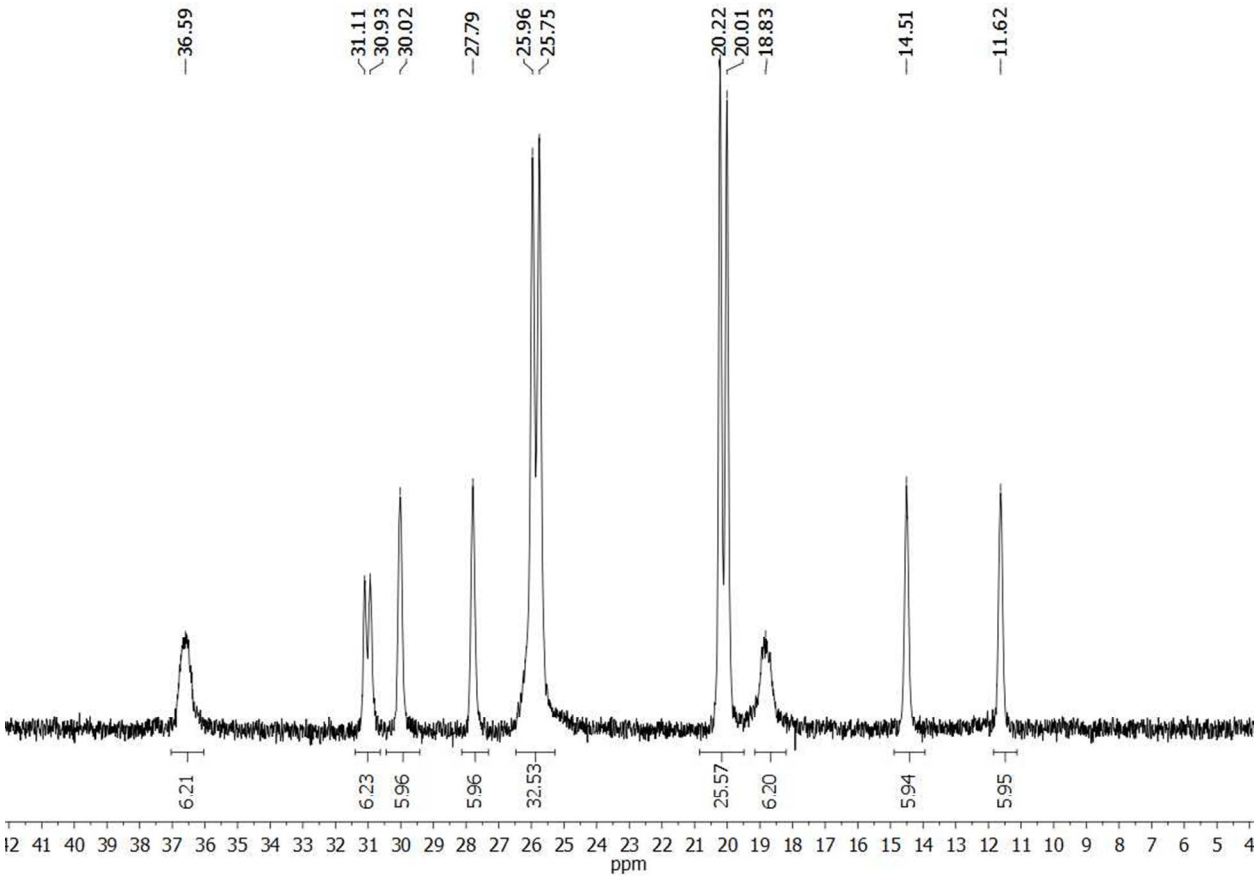

Figure S9. $^{31}P\{^{1}H\}$ NMR spectrum for protonation of $Fe_2(pdt)(CO)_2(PMe_3)_4$ with one equiv of $H(OEt_2)_2BAr^F{}_4$ at -60 °C in CD_2Cl_2 solution. Only two species are now present in solution: [μ-H**2**]$^+$ and [*t*-H**2**]$^+$ in a 2:1 ratio.

Assignments: The doublets centered at δ 25.0 and 19 are assigned to [μ-H**2**]$^+$. Signals centered at δ 35.9, 30.3 and 17.9 are assigned to [*t*-H**2**]$^+$, a fourth signal is present at δ 25.32 but partially obscured by the [μ-H**2**]$^+$ signal centered at δ 25.0.

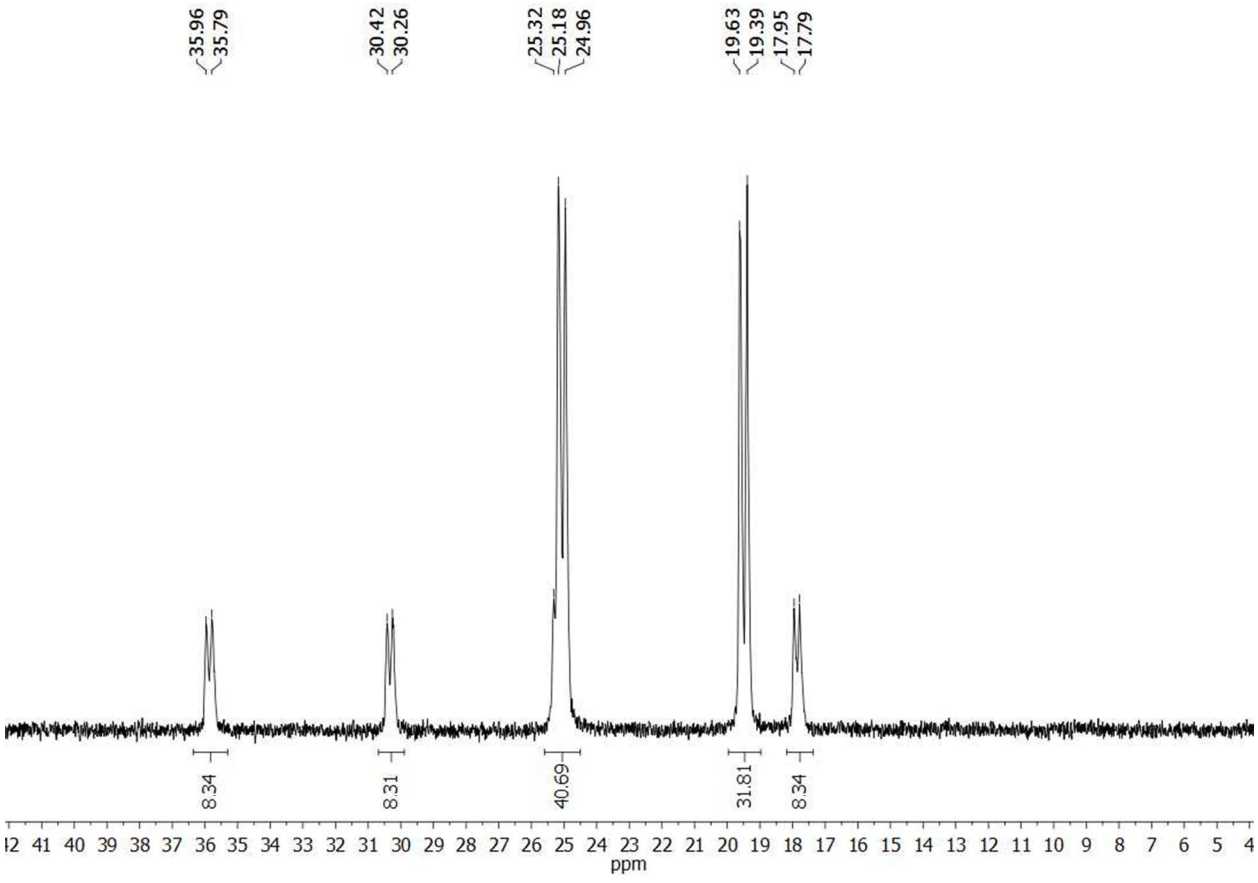

Figure S10. ^{1}H NMR spectra for protonation of $Fe_2(pdt)(CO)_2(PMe_3)_4$ with one equiv of $H(OEt_2)_2BAr^F{}_4$ at -90 (bottom) followed by warming the sample to -60 °C (top), recorded on CD_2Cl_2 solutions.

Assignments: The triplet of triplets at δ -18.8 (J_{PH} = 27.2, 3.4 Hz) is assigned to the bridging hydride [μ-H**2**]$^+$. The doublet of doublets centered at δ -2.2 (J_{PH} = 57, 101 Hz) is assigned to [*t*-H**2**]$^+$. The doublet observed at δ 4.6 together with a doublet at δ 2.9 (bottom indicated with *) are tentatively assigned to the *S*-protonated dithiolate.

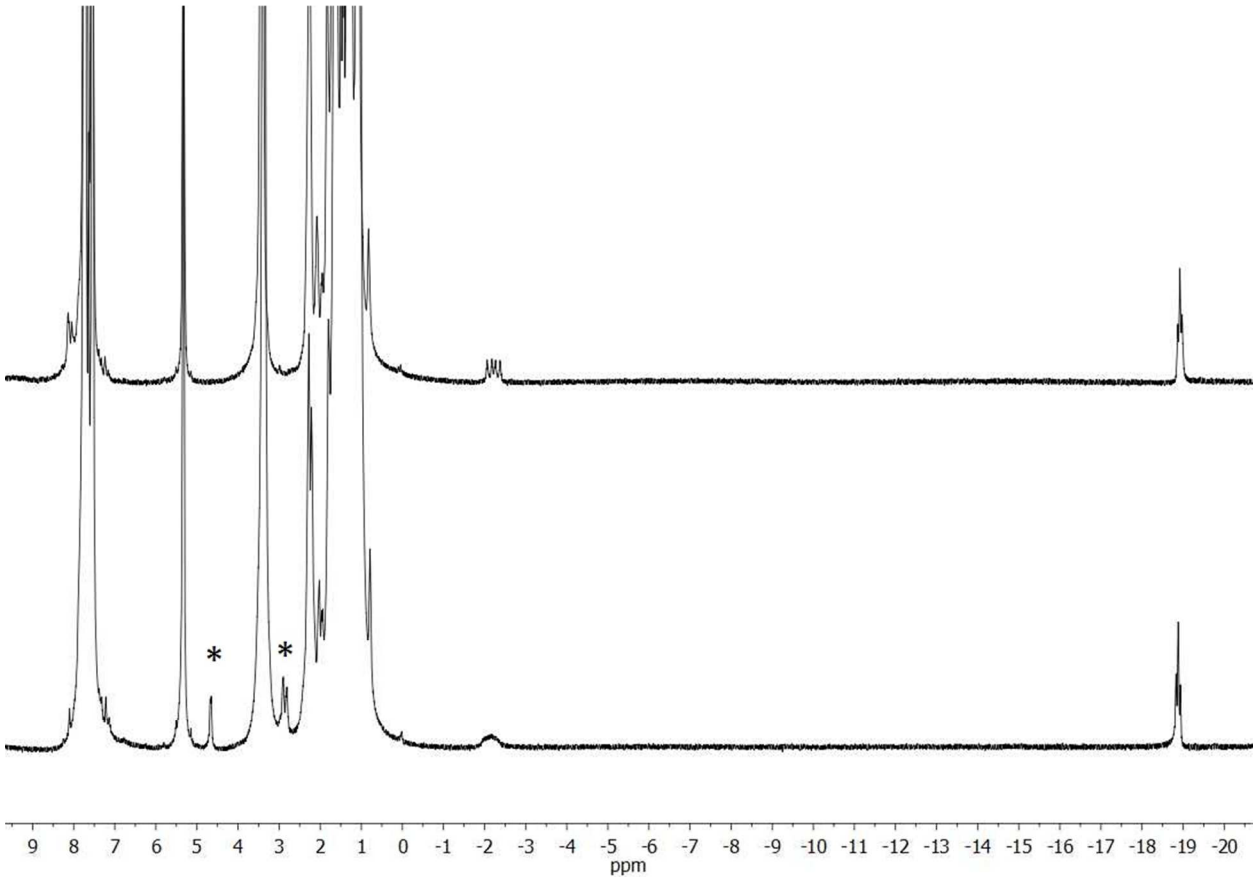

Analysis of the kinetics for the protonation of 2.

The results of several experiments, summarized in Figure 6. In these experiments, the starting concentration [**2**] was held constant and the amount of acid ($H(OEt_2)_2BAr^F{}_4$) was varied up to 1 equiv.

Procedure: Under inert atmosphere, into a 5 mL scintillation vial 8 mg of diiron compound were dissolved in 0.4 mL of CD_2Cl_2 at room temperature. In a separate vial the appropriate amount of ($H(OEt_2)_2BAr^F{}_4$) was weighted and dissolved in 0.3 mL of CD_2Cl_2 at room temperature. The solution of the acid was transferred with a pipet onto the diiron solution while swirling the vial. The resulting mixture was then rapidly transferred to a NMR tube, which was stored in a dry ice/acetone bath before the spectrum was recorded at room temperature.

The dependence of the product ratio vs equiv $H(OEt_2)_2BAr^F{}_4$ are consistent with pathways to [*t*-H**2**$^+$] and [μ-H**2**]$^+$ that are first and second order in [**2**], respectively:

$$-d[\mathbf{2}]/dt = k_t[H\mathbf{2}^+] + k_\mu[H\mathbf{2}^+][\mathbf{2}] = d[t\text{-}H\mathbf{2}^+]/dt + d[\mu\text{-}H\mathbf{2}^+]/dt$$

The rates of the first and second order pathways are abbreviated as follows:

$$d[t\text{-}H\mathbf{2}^+]/dt = r_t$$

$$d[\mu\text{-}H\mathbf{2}^+]/dt = r_\mu$$

The relative rates are reflected by the product ratio, i.e.,

$$r_\mu/r_t = \%[\mu\text{-}H\mathbf{2}^+]/\%[t\text{-}H\mathbf{2}^+]$$

as well as the ratio of the individual rate expressions:

$$r_\mu/r_t = k_\mu[H\mathbf{2}^+][\mathbf{2}]/k_t[H\mathbf{2}^+] = k_\mu[\mathbf{2}]/k_t$$

Thus, the relative rate constants can be deduced from the product ratio:

$$k_\mu[\mathbf{2}]/k_t = \%[\mu\text{-}H\mathbf{2}^+]/\%[t\text{-}H\mathbf{2}^+]$$

In this model, we assume that H^+ is quantitatively consumed by protonation at sulfur giving [H**2**$^+$]. The concentration of unprotonated diiron complex, [**2**], remains constant throughout the reaction. The product ratio r_μ/r_t is related to the rate constants:

$$(k_\mu/k_t)[\mathbf{2}] = \%[\mu\text{-}H\mathbf{2}^+]/\%[t\text{-}H\mathbf{2}^+]$$

The best fit straight line for %[μ-H**2**$^+$]/%[*t*-H**2**$^+$] vs equiv [**2**] (unprotonated) has a slope of 14.4, which is assigned as k_μ/k_t.

Figure S11. IR spectrum of the CO region for a CH_2Cl_2 solution of $Fe_2(pdt)(CO)_2(PMe_3)_4$. *Observed:* υ_{CO} = 1857 and 1836 cm^{-1}.

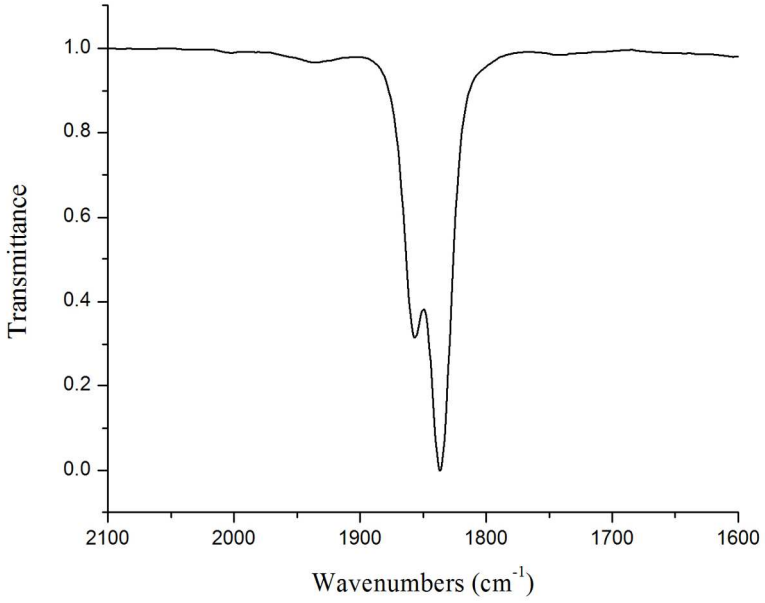

Table S1. IR data for Selected Diiron Hydrides.

Compound	**ν_{CO} (solution)**	**solvent**
$[\mu\text{-}HFe_2(edt)(CO)_4(PMe_3)_2]^+$	2034(s), 1994(s)	MeCN[21]
$[\mu\text{-}HFe_2(edt)(CO)_2(PMe_3)_4]^+$ ($[\mu\text{-}H\mathbf{1}]^+$)	1940, 1928	CH_2Cl_2
$[\mu\text{-}HFe_2(pdt)(CO)_4(PMe_3)_2]^+$	2029(s), 1989(s)	MeCN[21]
$[\mu\text{-}HFe_2(pdt)(CO)_2(PMe_3)_4]^+$ ($[\mu\text{-}H\mathbf{2}]^+$)	1944, 1933	CH_2Cl_2
$[t\text{-}HFe_2(adt)(CO)_2(PMe_3)_4]^+$ ($[t\text{-}H\mathbf{3}]^+$)	1945 (m), 1879 (s)	CH_2Cl_2
$[t\text{-}HFe_2(pdt)(CO)_2(dppv)_2]^+$	1965, 1905[8]	CH_2Cl_2
$[\mu\text{-}HFe_2(pdt)(CO)_2(dppv)_2]^+$	1958[8]	CH_2Cl_2

Figure S12. IR of the CO region for a CH_2Cl_2 solution of $Fe_2(pdt)(CO)_2(PMe_3)_4$ with one equiv of $H(OEt_2)_2BAr^F{}_4$ at various times.
Assignments: Two species are present in solution: $[t\text{-H}\mathbf{2}]^+$ υ_{CO} 1944 and 1883 cm^{-1}, band at 1850 cm^{-1} is attributed to υ_{FeH} and $[\mu\text{-H}\mathbf{2}]^+$ υ_{CO} 1944 and 1933 cm^{-1}.

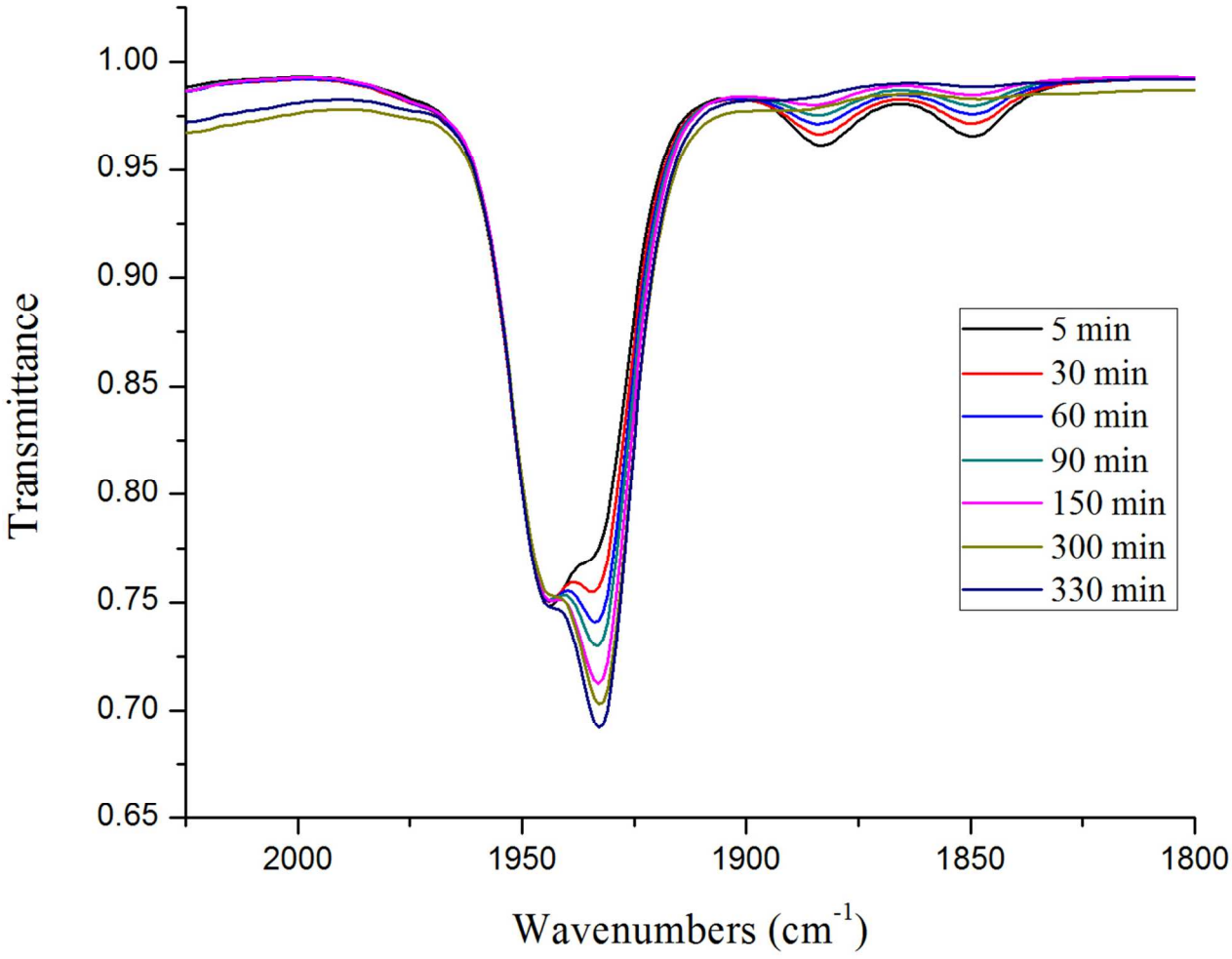

Figure S13. IR spectra of the CO region for a CH_2Cl_2 solution of $Fe_2(pdt)(CO)_2(PMe_3)_4$ with one equiv of $D(OEt_2)_2BAr^F{}_4$ (black) and for a CH_2Cl_2 solution of $Fe_2(pdt)(CO)_2(PMe_3)_4$ with one equiv of $H(OEt_2)_2BAr^F{}_4$.
Assignments: υ_{CO} for [*t*-D**2**]$^+$ 1944 and 1866 cm^{-1}. υ_{CO} for [μ-D**2**]$^+$ 1944 and 1933 cm^{-1}. The weak signal at ~1830 cm^{-1} is unassigned. The assignments are tentative, pending further analysis.

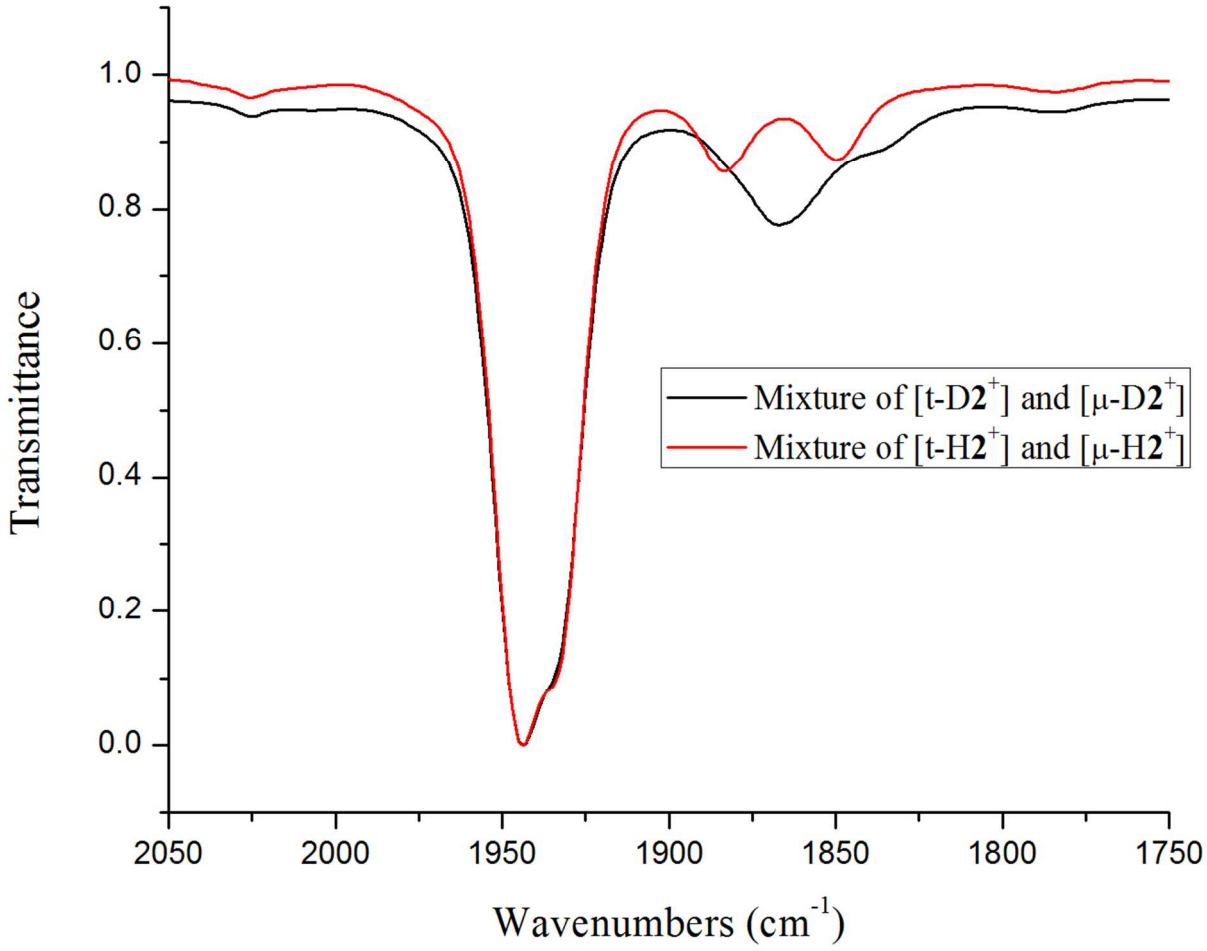

Figure S14. Rate of isomerization from [*t*-H**2**]$^+$ to [μ-H**2**]$^+$ measured by monitoring the disappearance of NMR resonance for the terminal hydride in a CD_2Cl_2 solution over time, at 20 °C. Isomerization was found to follow a first order kinetic. The equilibrium constant at 20 °C was found to be $8 \cdot 10^{-5}$ s^{-1}.

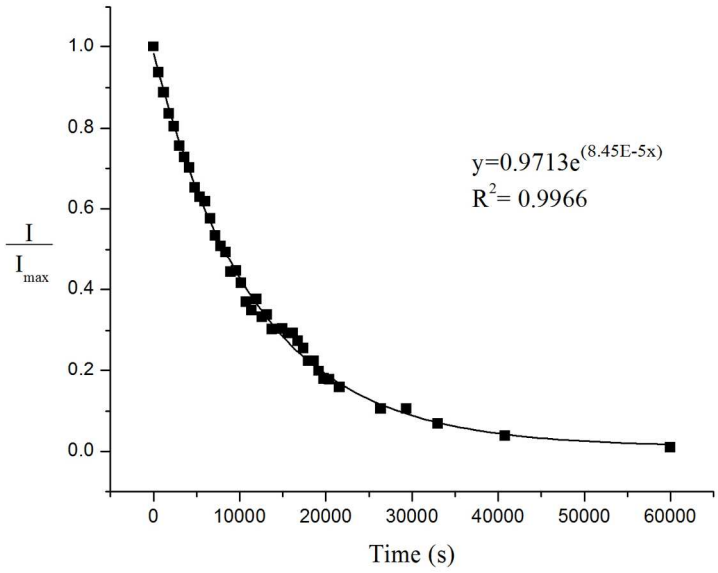

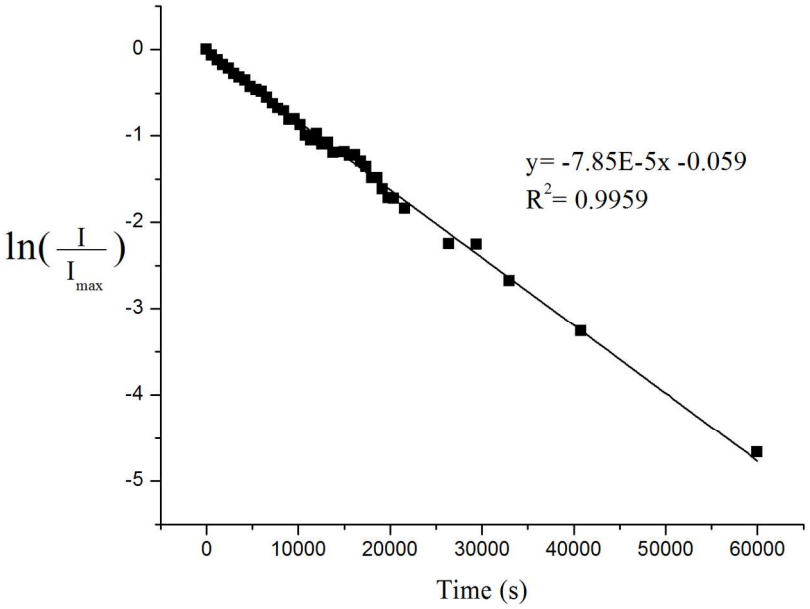

Figure S15. ^{1}H NMR spectrum for protonation of a 1:1 mixture (CD_2Cl_2 solution) of $Fe_2(edt)(CO)_2(PMe_3)_4$ and $Fe_2(pdt)(CO)_2(PMe_3)_4$ with one equiv of $H(OEt_2)_2BAr^F{}_4$ at -90 °C (bottom). ^{1}H NMR spectrum for protonation of a CD_2Cl_2 solution of $Fe_2(pdt)(CO)_2(PMe_3)_4$ treated with 0.5 equiv of $H(OEt_2)_2BAr^F{}_4$ at -90 °C (top).

Assignments: Resonance for [*t*-H**2**]$^+$ at δ -2.1; [μ-H**2**]$^+$ at δ -19.08; [μ-H**1**]$^+$ at δ -20.77.

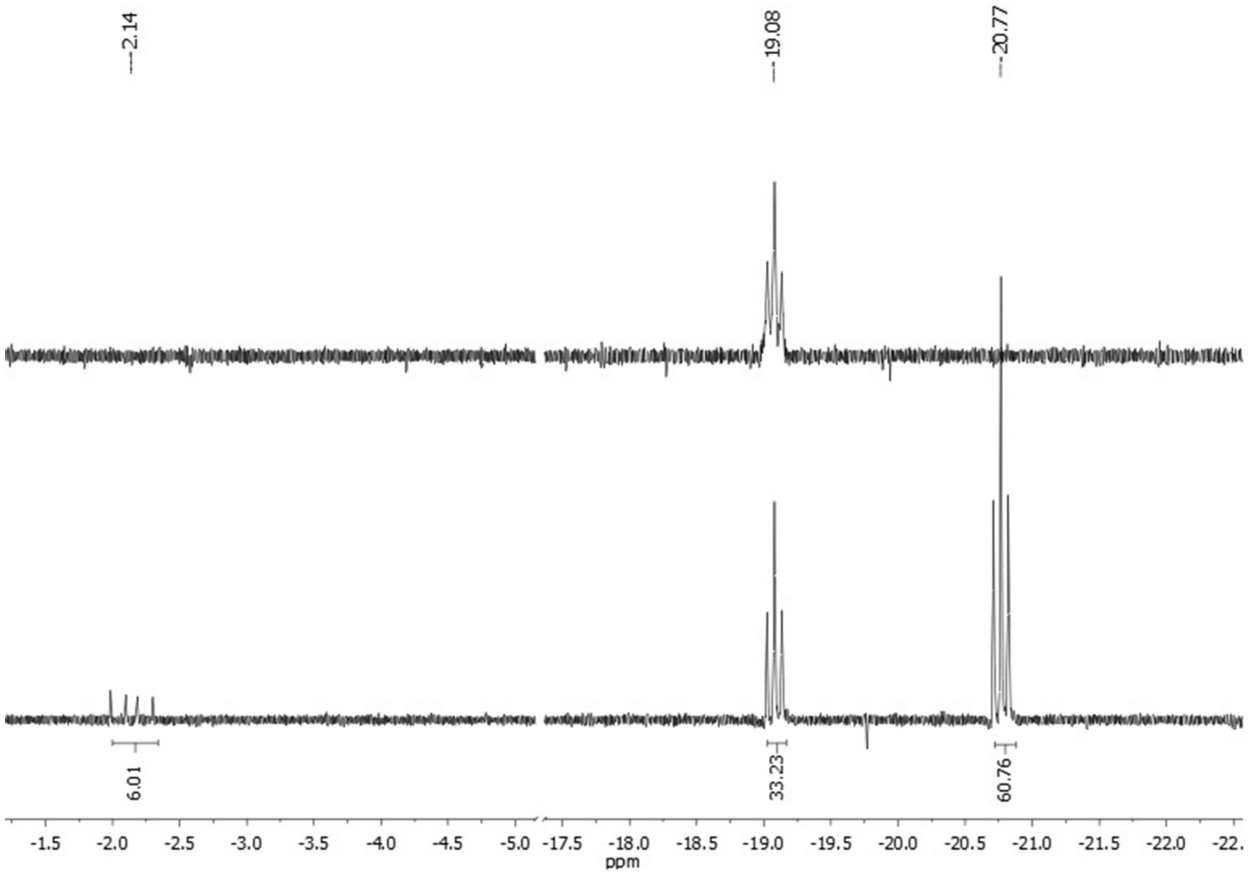

$Fe_2(adt)(CO)_6$. The following procedure is a modification of the published procedure (Li, H.; Rauchfuss, T. B. *J. Am. Chem. Soc.* **2002**, *124*, 726.). A 500-mL Schlenk flask equipped with a dropping funnel was dissolved 3.00 g (8.72 mmol) of $Fe_2S_2(CO)_6$ in 100 mL of THF. This red-orange homogeneous solution was cooled to -78 °C. The dropping funnel was charged with 20 mL of THF followed by 17.88 mL (17.87 mmol, 2.05 equiv) of 1M solution of $LiBHEt_3$ in THF. The hydride solution was added to the reaction over the course of 20 min to afford a dark green solution. After the addition was complete, the reaction mixture was stirred for an additional 20 min. The reaction temperature was allowed to slowly rise to -30 °C, which caused the color to change from deep green to deep red. After 10 min. of stirring at -30 °C, the reaction mixture was cooled again to - 78 °C. The addition funnel was charged with 15 mL of THF and 1.4 mL (18.31 mmol, 2.10 equiv) of CF_3CO_2H. This solution was added to the reaction flask over 20 min. During this addition the color changed from deep red to deep green, then to deep red again and finally to a red-orange clear solution. To this solution was added 1.223 g (8.72 mmol) of hexamethylenetetramine, which had been finely ground and subsequently vacuum-dried. This mixture was allowed to warm to room temperature while stirring. The reaction was stirred for 28 h before solvent was removed in vacuo to afford a dark red/black gummy residue. The residue was then extracted with ca. 100 mL of CH_2Cl_2, and this extract was passed though a plug of silica gel. Solvent was evaporated under vacuum, and the residue was extracted in minimal amount of a pentane/CH_2Cl_2 mixture (8:2, *ca.* 20 mL is required). This extract was chromatographed on a 5 x 25 cm column of silica gel eluting with pentanes to remove two red orange undefined products. The polarity of the eluting solvent was then increased to pentane/CH_2Cl_2 mixture (9:1), then increased to pentane/CH_2Cl_2 mixture (7:3) to afford the product as bright red colored solid. Yield: 1.3 g (38.5%). IR (pentanes): 2075, 2035, 2007, 1990, 1980 cm^{-1} (see Lawrence, J. D.; Li, H.; Rauchfuss, T. B.; Bénard, M.; Rohmer, M.-M. *Angew Chem., Int. Ed.* **2001**, *40*, 1768).

Figure S16. ^{1}H NMR spectrum of a CD_2Cl_2 solution of crude $Fe_2(adt)(PMe_3)_4(CO)_2$ at -30 °C.

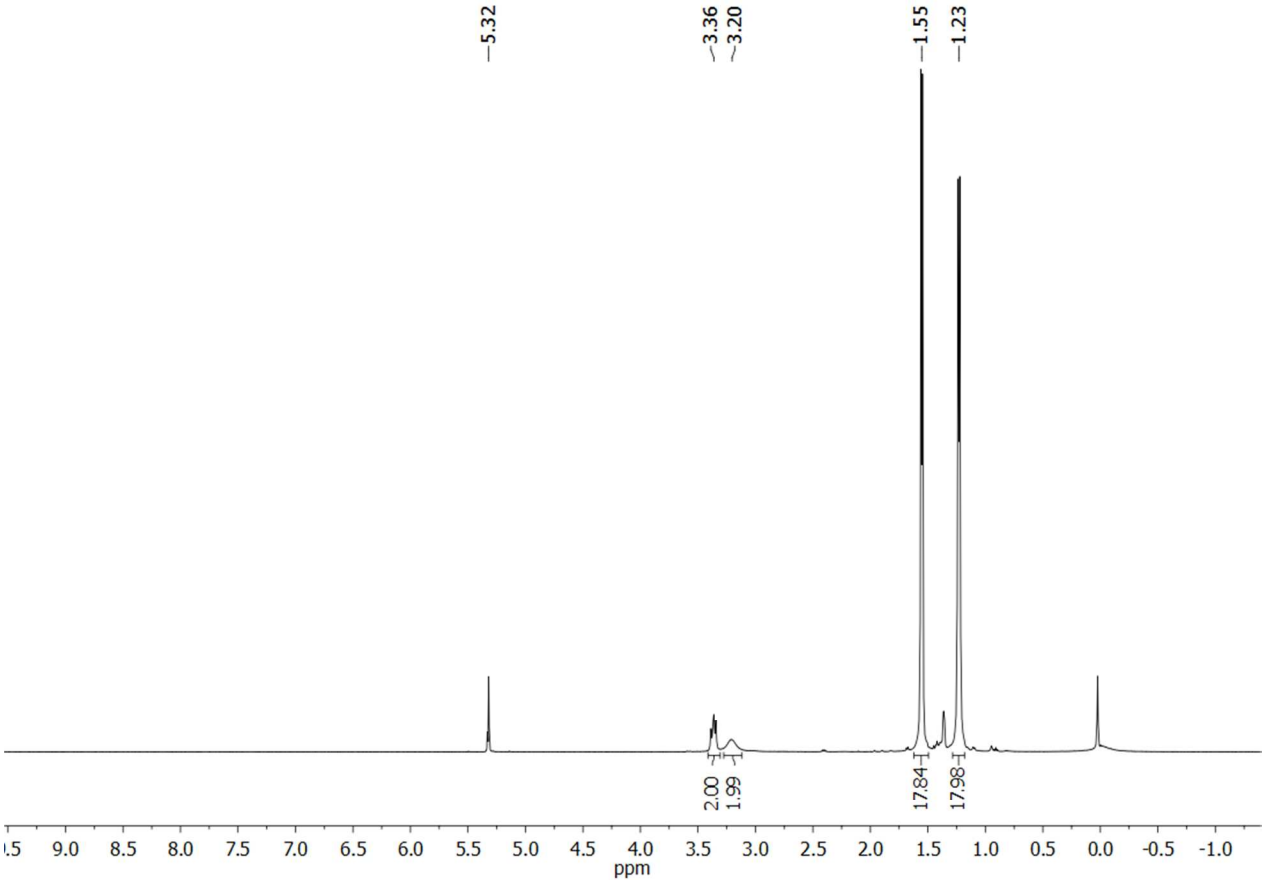

Figure S17. $^{31}P\{^{1}H\}$ NMR spectrum of a CD_2Cl_2 solution of crude $Fe_2(adt)(CO)_2(PMe_3)_4$ (**3**) at -30 °C.

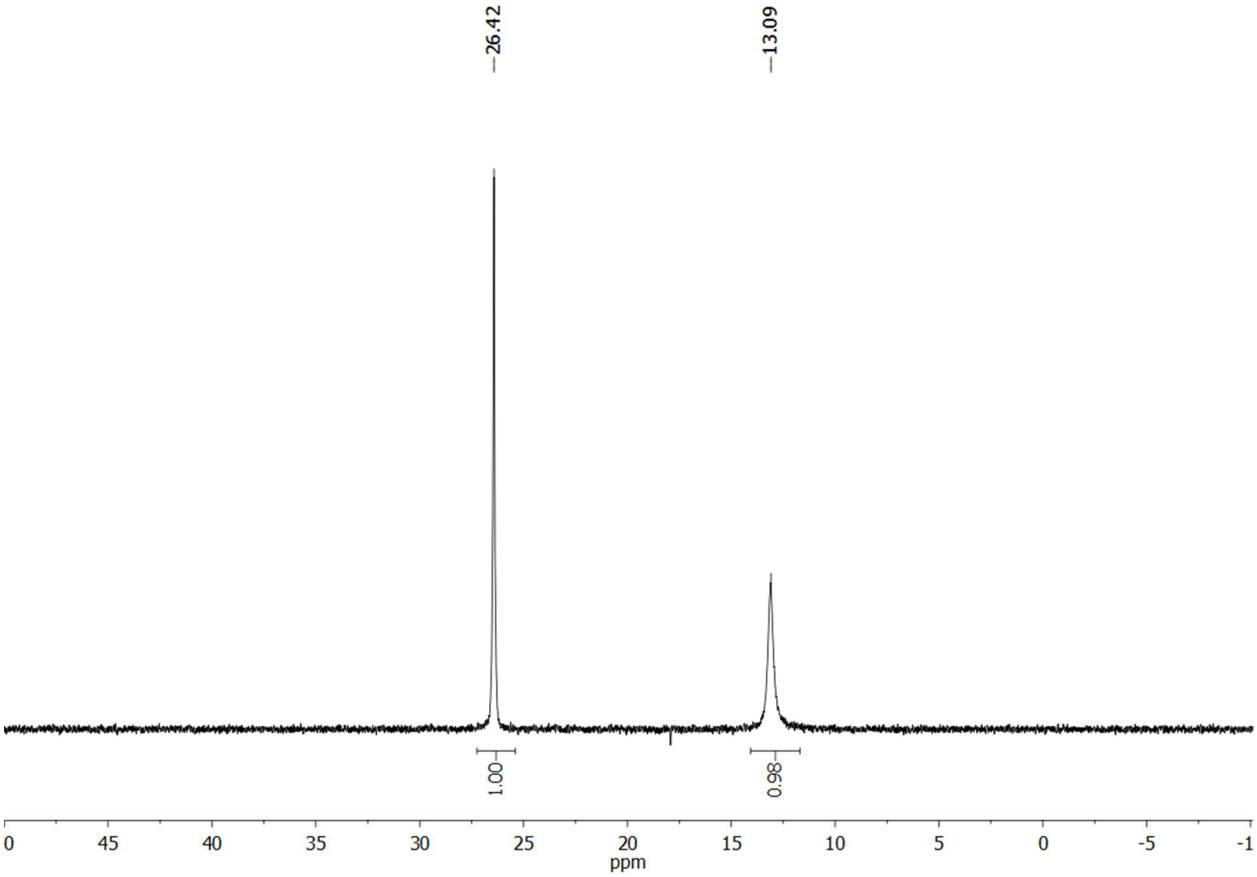

Figure S18. ^{31}P $\{^{1}H\}$ NMR spectrum of a CD_2Cl_2 solution of $Fe_2(adt)(CO)_2(PMe_3)_4$: starting from the bottom -90, -50, and -10 °C. A small amount of unidentified impurity is apparent at δ 26.1.

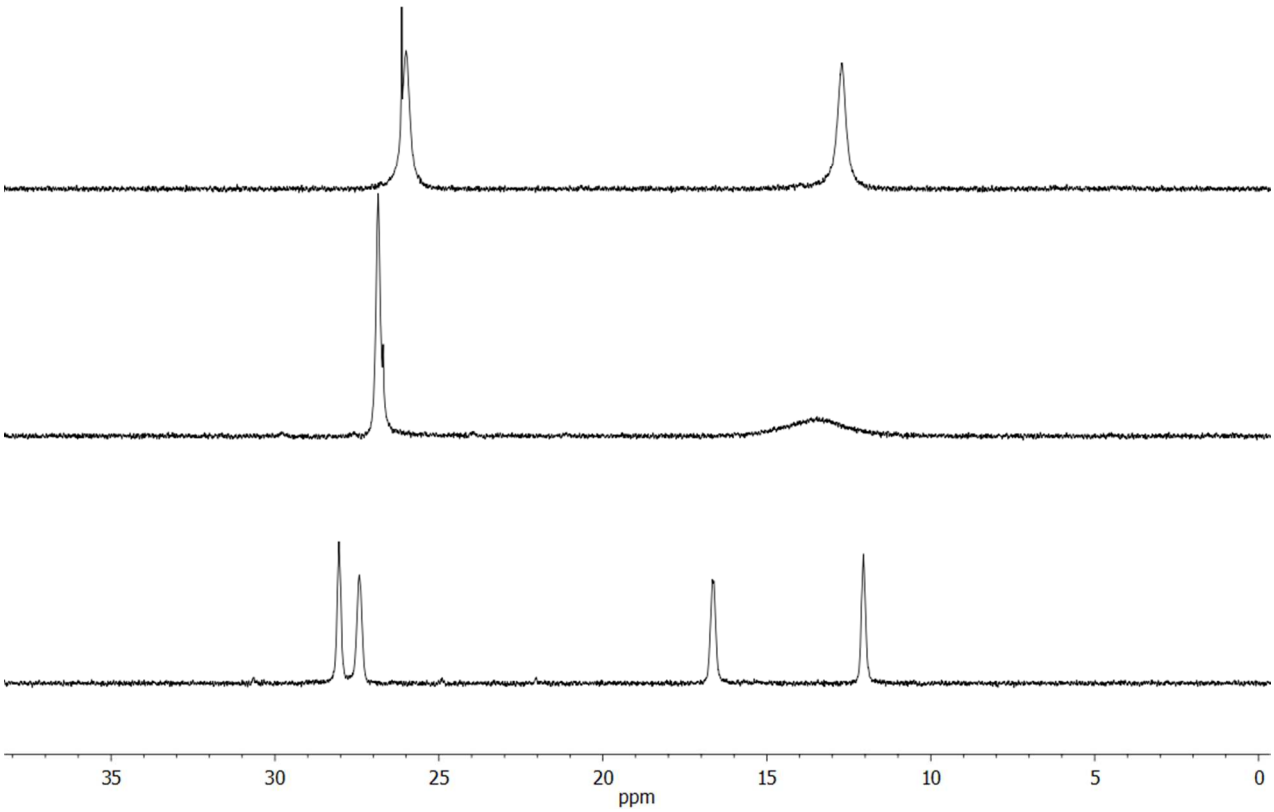

Figure S19. Cyclic voltammogram of $Fe_2(adt)(CO)_2(PMe_3)_4$ in 1,2-difluorobenzene referenced to Fc/Fc^+.

Conditions and Results: complex = 1 mM; $[TBA]PF_6$ = 100 mM; $E_{½}$ = -920 mV (i_{pa}/i_{pc} = 0.61).

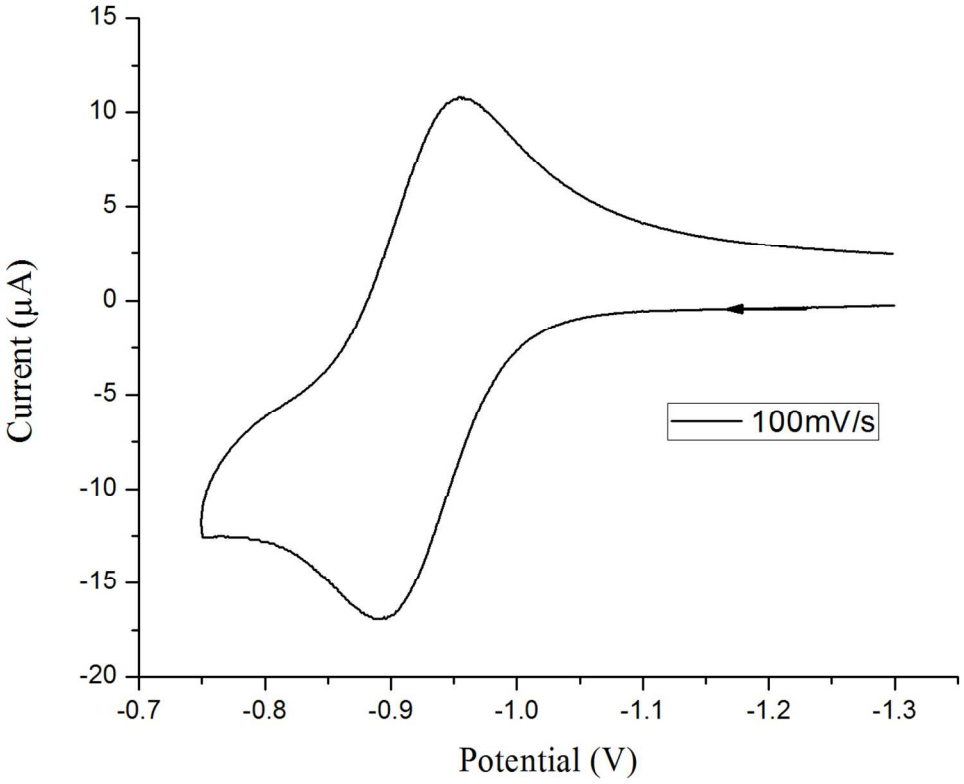

Figure S20. IR spectrum in the CO region for a CH_2Cl_2 solution of $Fe_2(adt)(CO)_2(PMe_3)_4$. *Assignments:* υ_{CO} = 1860 and 1839 cm^{-1}. The band at 1804 cm^{-1} is an undefined impurity.

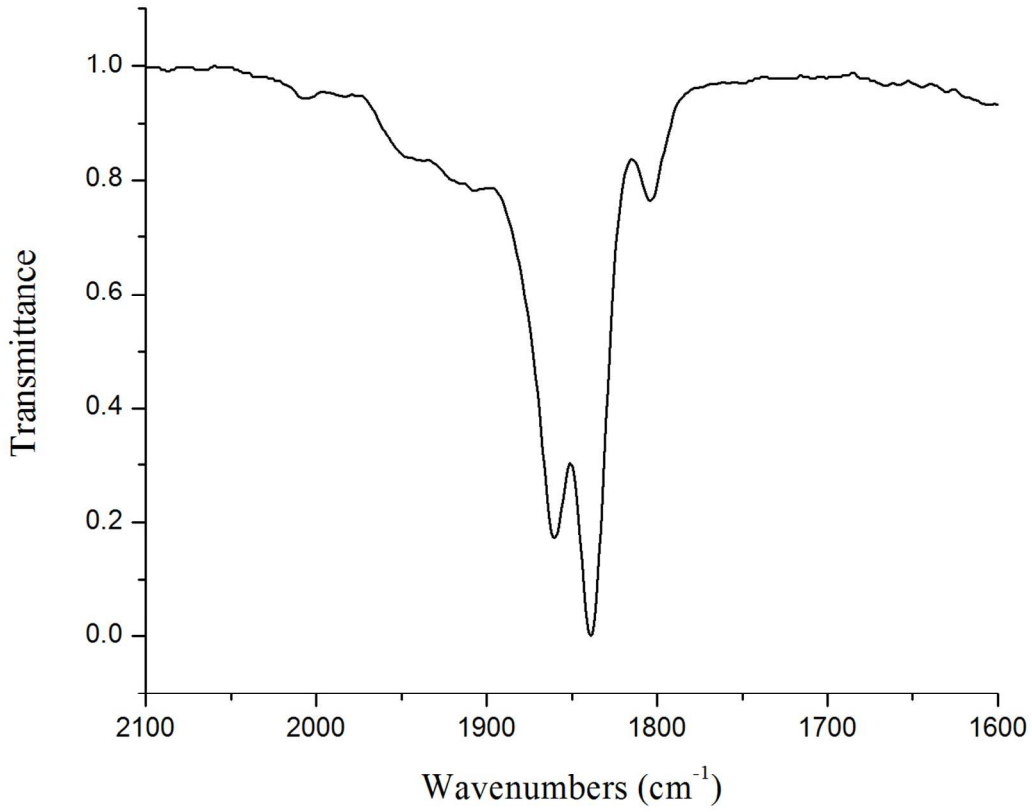

Figure S20. ^{1}H NMR spectrum of a CD_2Cl_2 solution of [*t*-H**3**]$^{+}$, the unsym isomer of $[HFe_2(adt)(PMe_3)_4(CO)_2]BAr^F{}_{20}$.

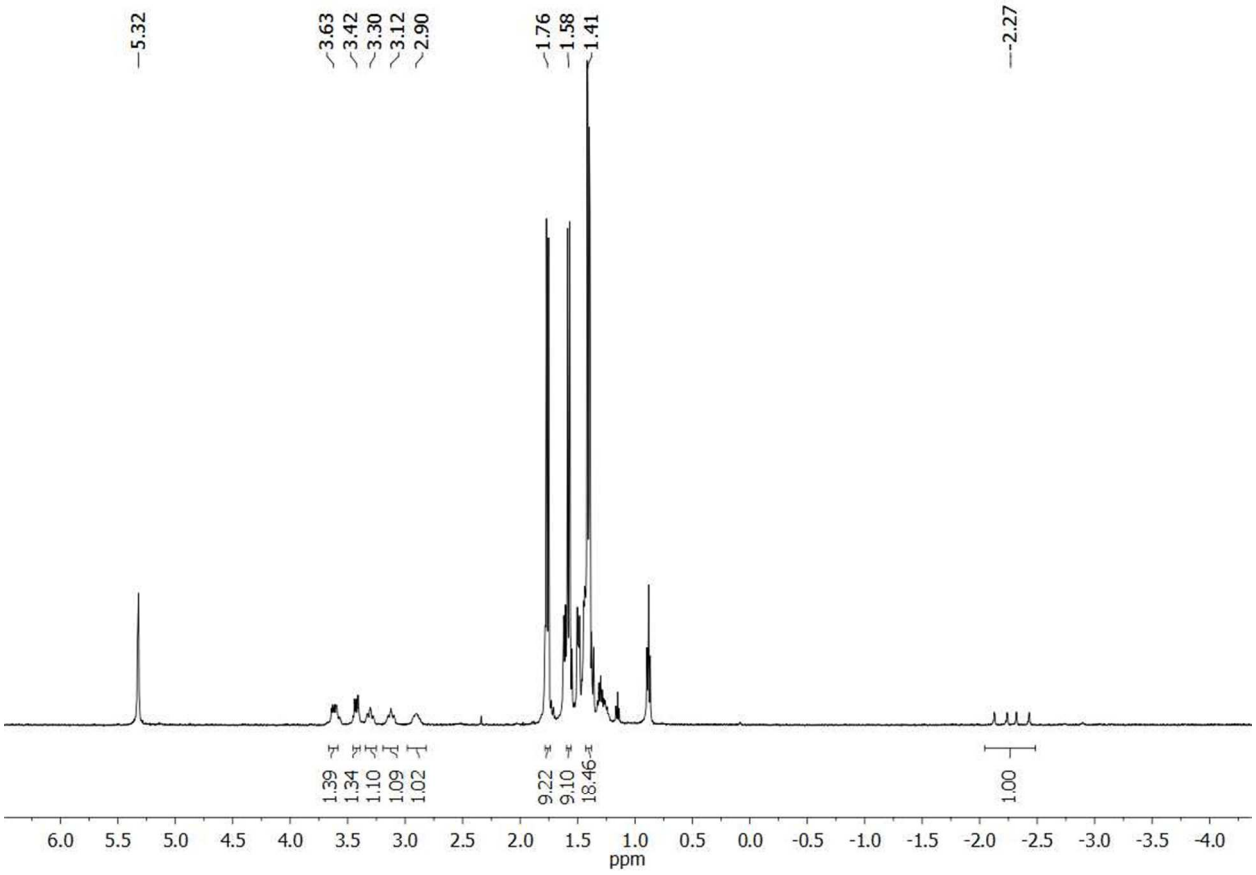

.

Figure S21. $^{31}P\{^{1}H\}$ NMR spectrum of a CD_2Cl_2 solution of $[HFe_2(adt)(PMe_3)_4(CO)_2]BAr^F{}_{20}$.

Assignments: The main isomer in solution is [*t*-H**3**]$^+$ at δ 31.62, 22.97, 21.21 and 12.41. Signals at δ 23.58 and 7.90 are for the isomeric compound [*t*-H**3'**]$^+$.

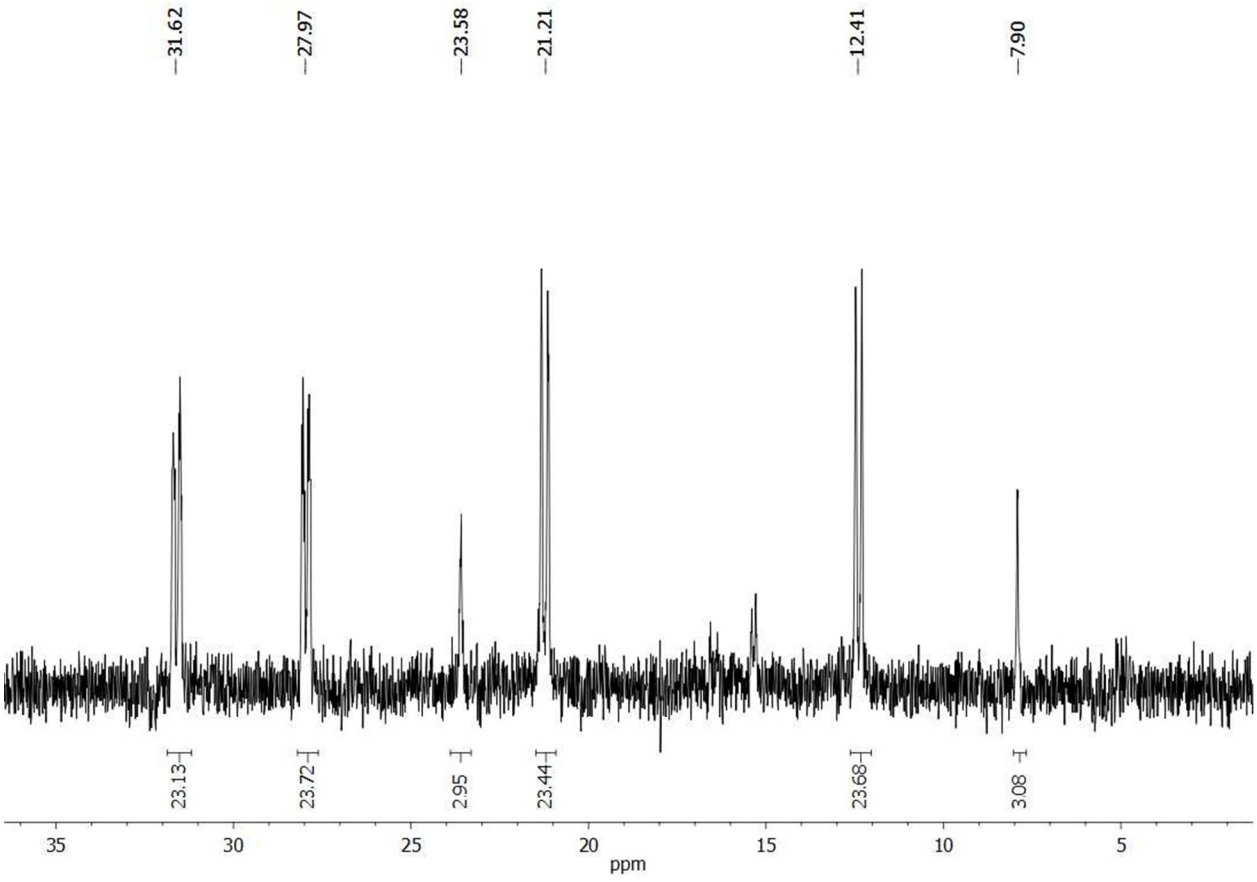

Figure S20. IR spectra of the CO region for a CH_2Cl_2 solution of $[HFe_2(adt)(PMe_3)_4(CO)_2]BAr^F{}_4$. On the basis of NMR analysis, the solution contains mostly [*t*-H**3**]$^+$ (95%) and [*t*-H**3'**]$^+$ (5%).

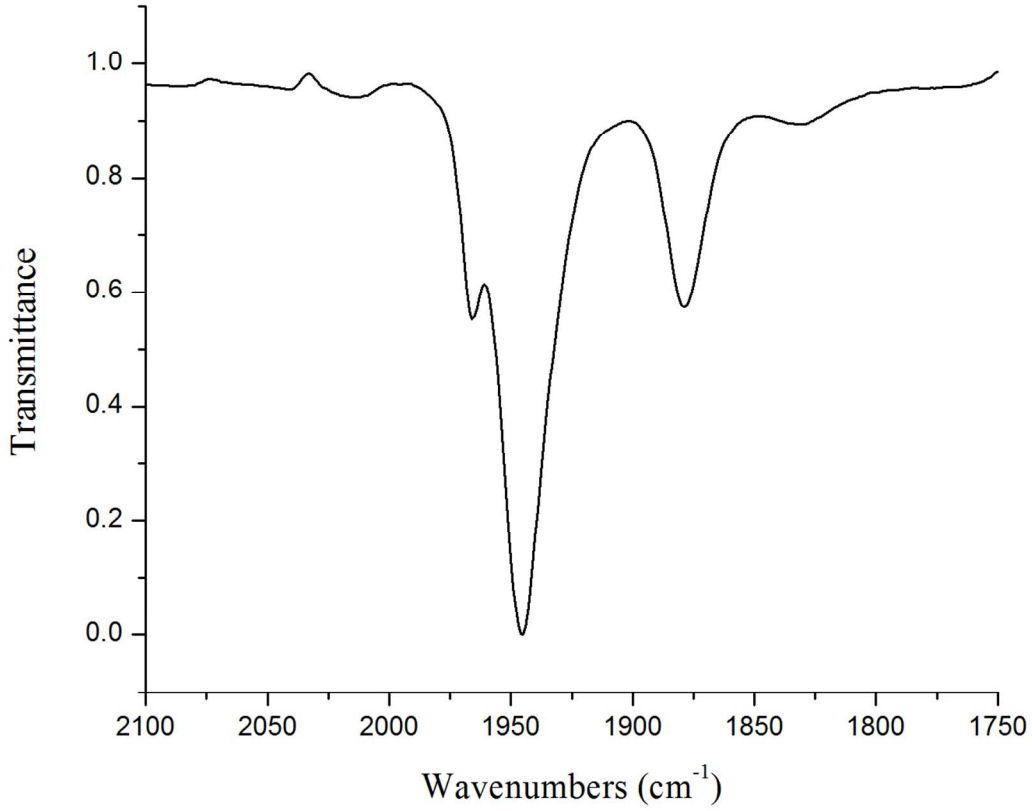

Figure S22. Rate of isomerization from $[t\text{-H}\mathbf{3}]^+$ to $[\mu\text{-H}\mathbf{3}]^+$ measured by monitoring the disappearance of terminal hydride resonance from ^{1}H NMR spectrum of a CD_2Cl_2 solution over time, at 20 °C. Isomerization was found to follow a first order kinetics. The rate constant at 20 °C was found to be $4.73 \cdot 10^{-5}$ s^{-1}.

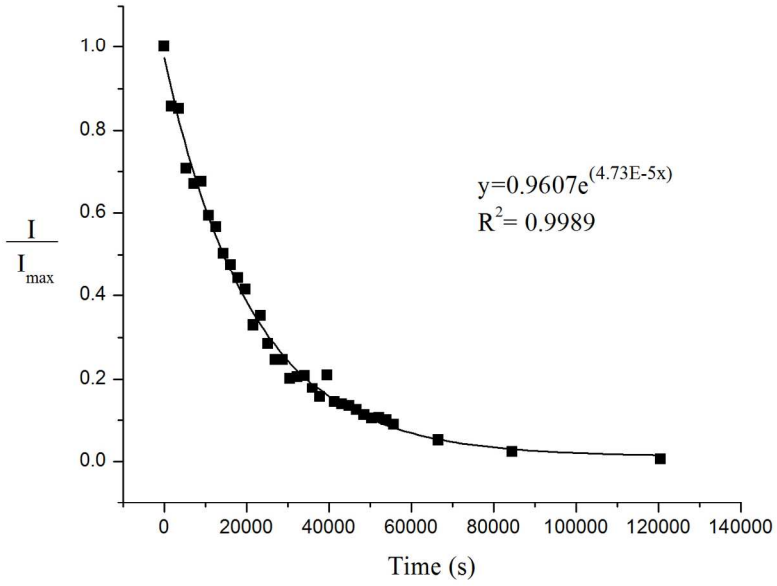

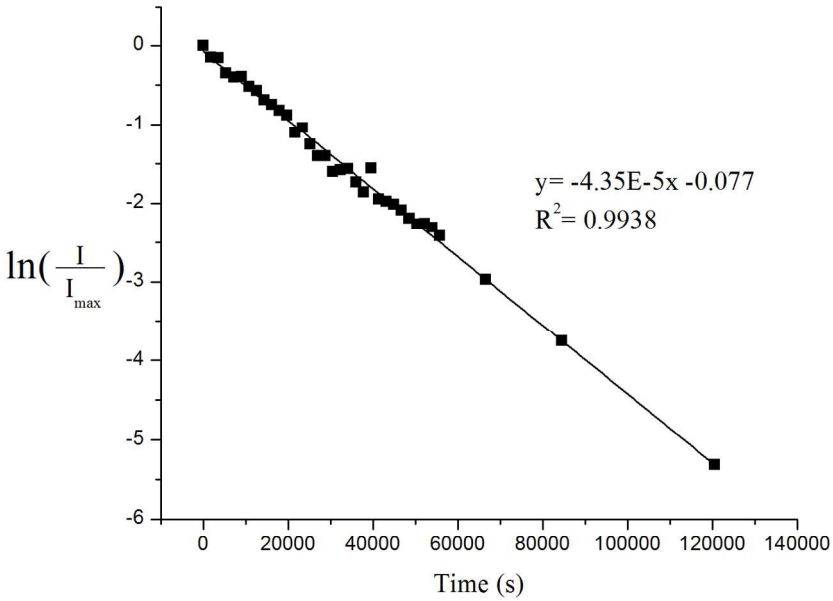

Figure S23. ^{1}H NMR spectrum (CD_2Cl_2 solution) for isomerization of [*t*-H**3**][BAr^F_{20}] to [μ-H**3**][BAr^F_{20}] at the starting time (bottom) and towards the end of the isomerization (top). Integrals are referenced to the solvent peak, which is set to 100.

Assignments: The signal at δ -2.25 is assigned to [*t*-H**3**][BAr^F_{20}]; signal at δ -2.86 is assigned to [*t*-H**3'**][BAr^F_{20}], and the signal at δ -18.74 [μ-H**3**][BAr^F_{20}]. Notice that [*t*-H**3**]$^+$ isomerizes faster than does [*t*-H**3'**]$^+$.

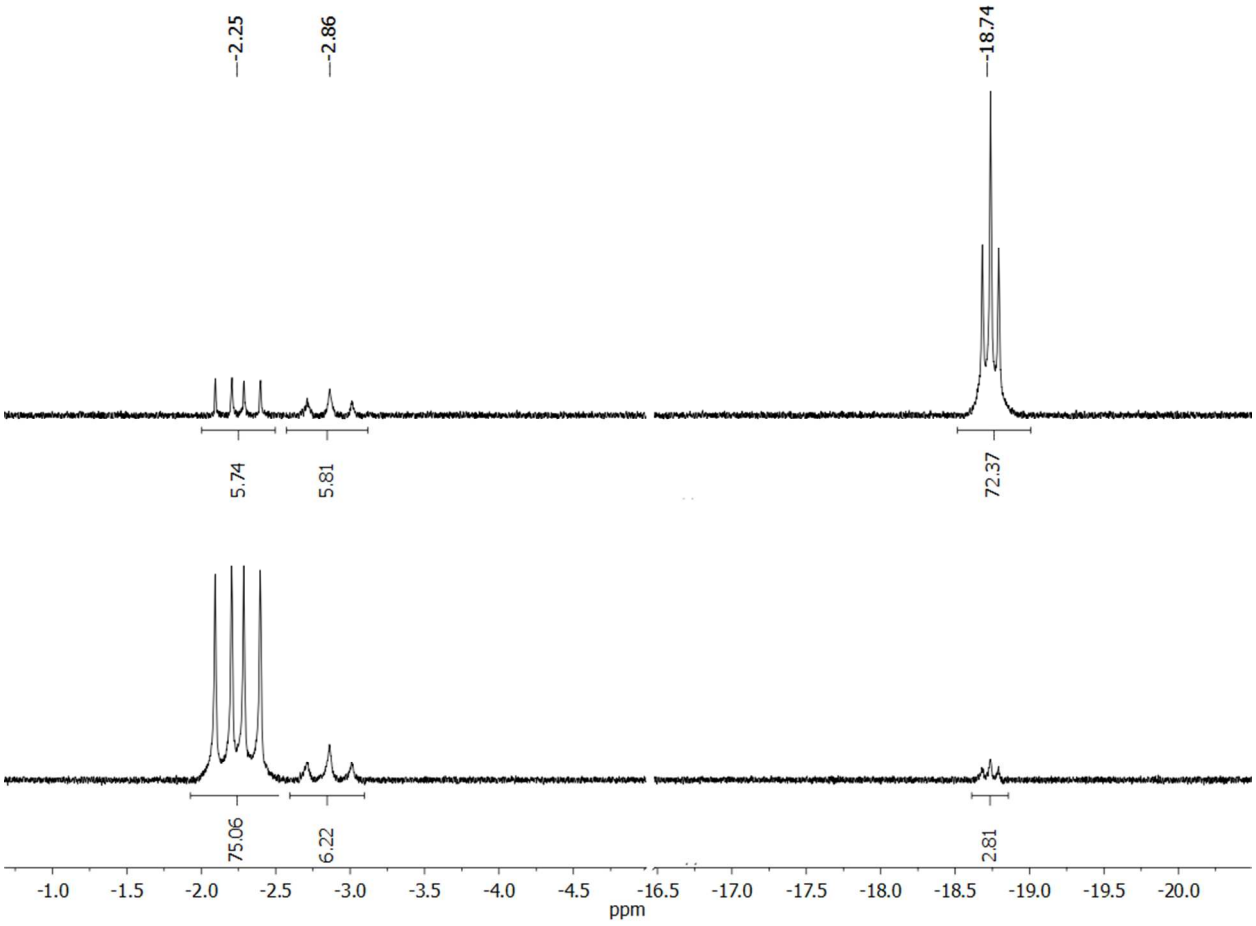

Figure S24. 1-D nOe ^{1}H NMR spectrum of a CD_2Cl_2 solution of [*t*-H**3**][BAr^{F}_{20}] at -10 °C involving irradiation at δ -2.29 and showing enhancement of N*H*, two P(CH_3)$_3$ signals, and some of the CH_2 groups.

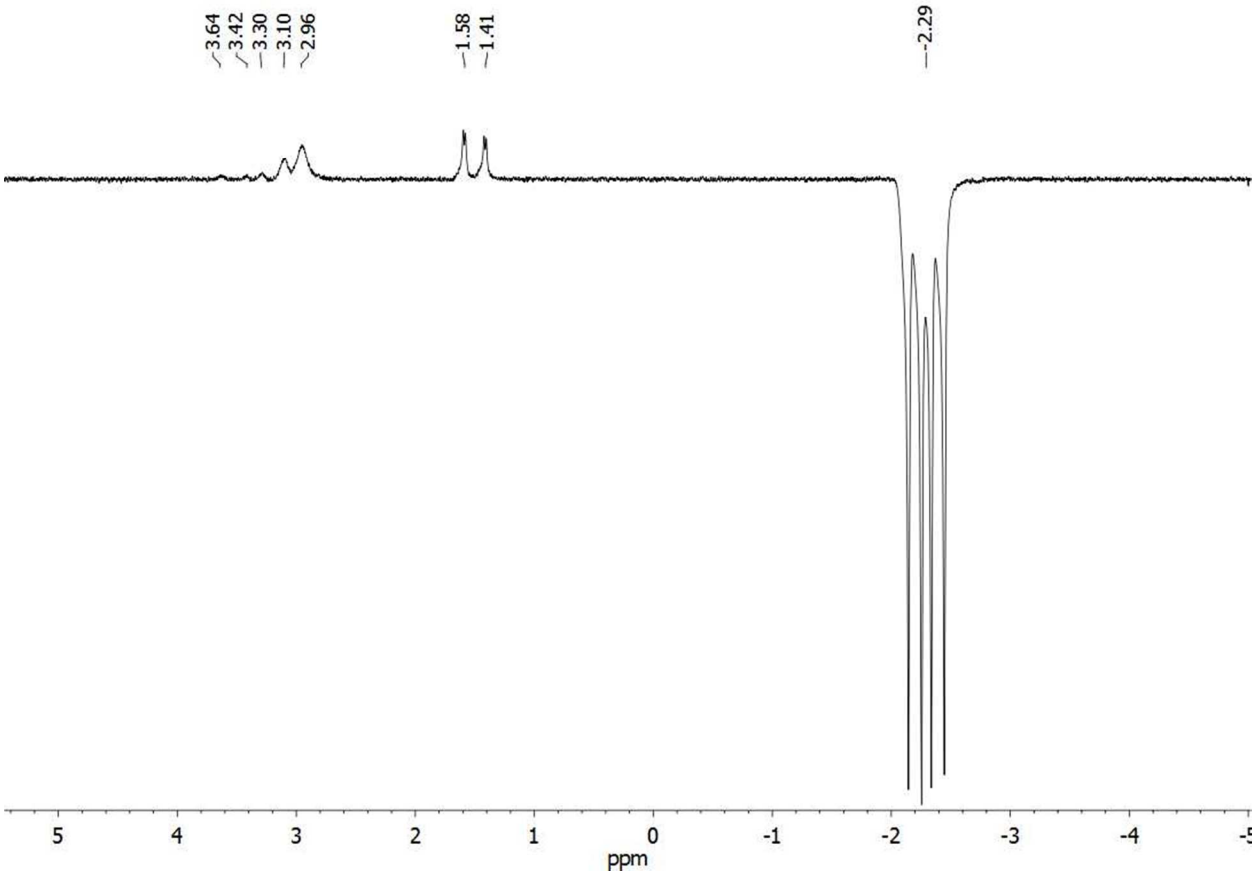

Figure S24. ^{1}H NMR spectrum of a CD_2Cl_2 solution of $[HFe_2(adt)(PMe_3)_4(CO)_2]BAr^F{}_4$ at -20 °C. The predominant isomer in solution is $[t\text{-H}\mathbf{3'}]^+$ (90%), and about 10% of $[t\text{-H}\mathbf{3}]^+$ is also present. The signals at low field are for $BAr^F{}_4^-$.

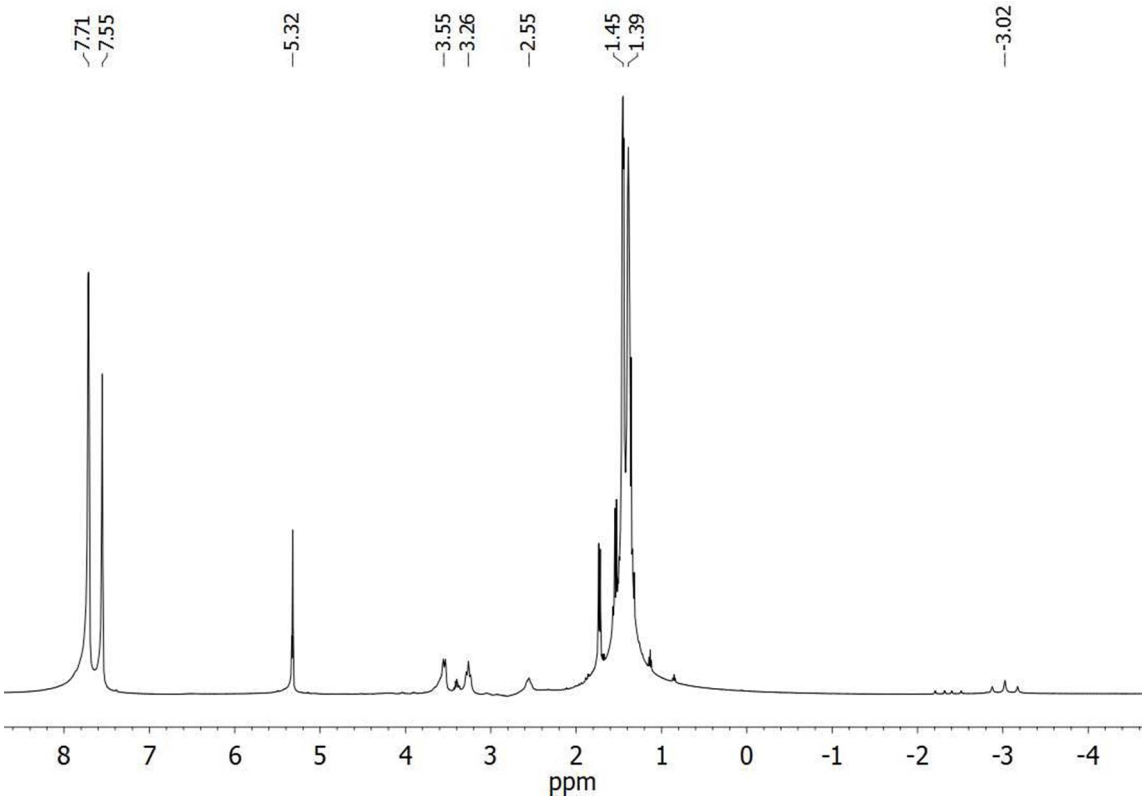

Figure S25. $^{31}P\{^{1}H\}$ NMR spectrum of a CD_2Cl_2 solution of $[HFe_2(adt)(PMe_3)_4(CO)_2]BAr^F{}_4$ at -20 °C. The main component in solution is [*t*-H**3'**]$^+$ (90%) with about 10% of the isomeric [*t*-H**3**]$^+$.

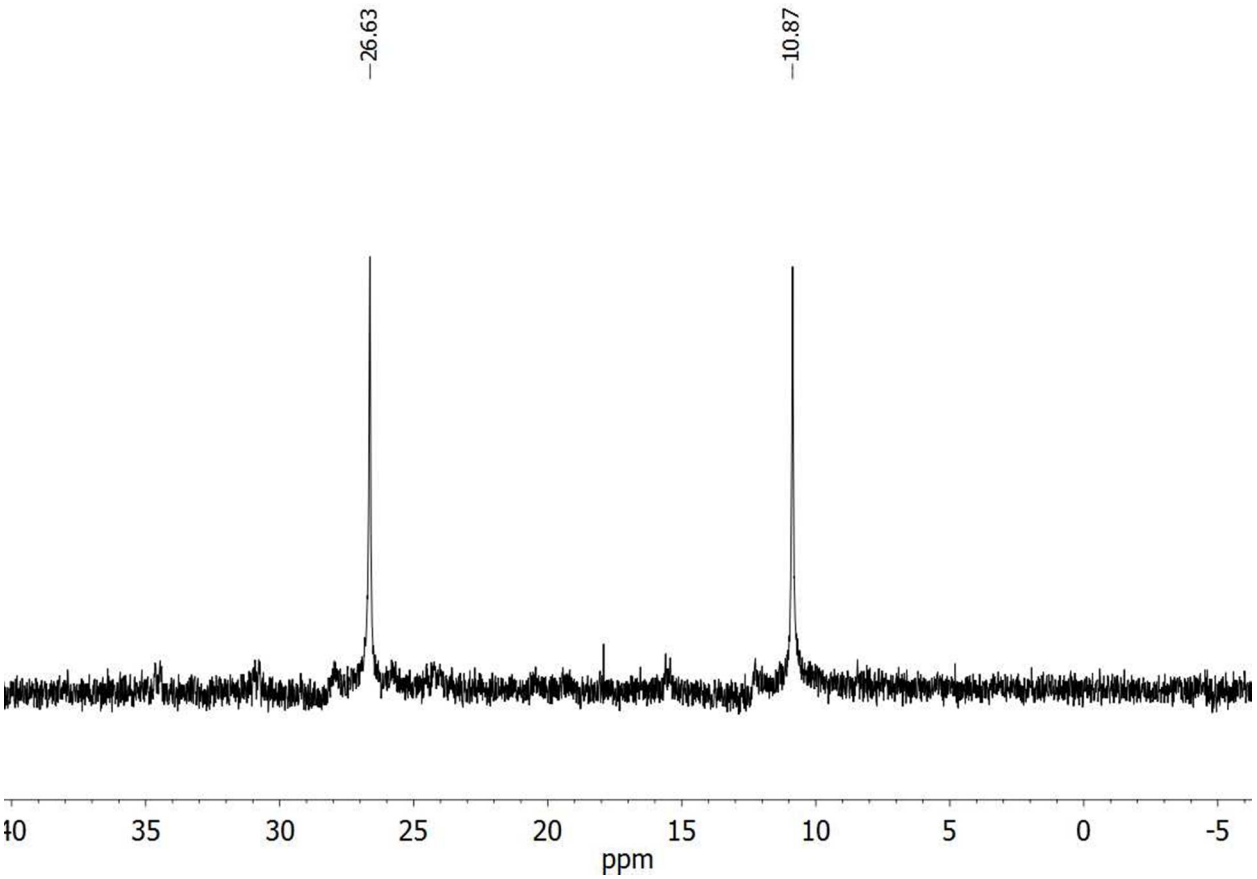

Figure S26. 1-D nOe ^{1}H NMR spectrum of a CD_2Cl_2 solution of [*t*-H**3'**][BAr^F_4] at -20 °C, involving irradiation at δ -3.02, showing enhancement of N*H* and P(CH_3)$_3$ signals.

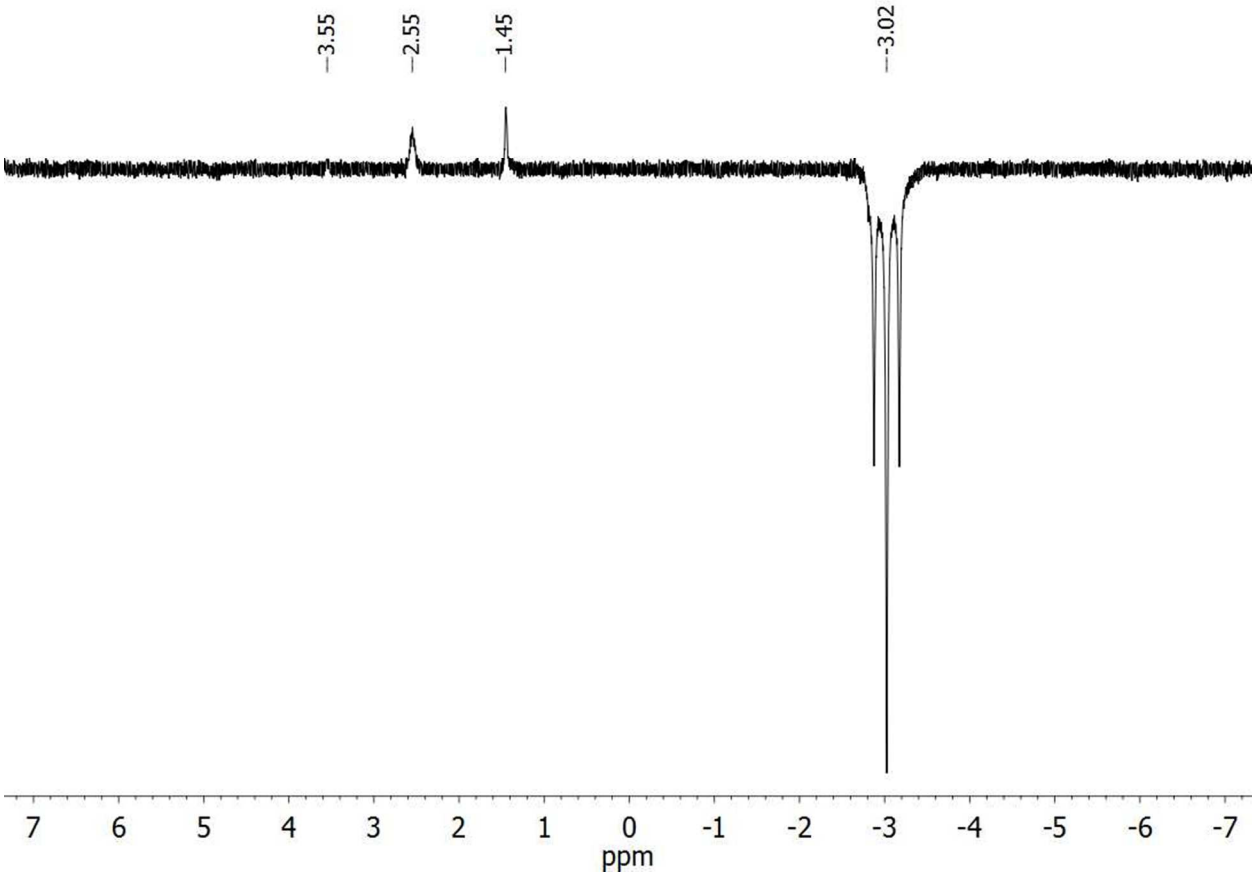

Figure S27. ^{1}H NMR spectrum (bottom) and NOESY1-D spectrum of the same involving irradiation at δ -3.02 all-basal isomer of $[HFe_2(adt)(PMe_3)_4(CO)_2]BAr^F{}_4$ ([*t*-H**3'**]$^+$) at -20 °C showing enhancement of N*H* and P(C*H*$_3$)$_3$ signals.

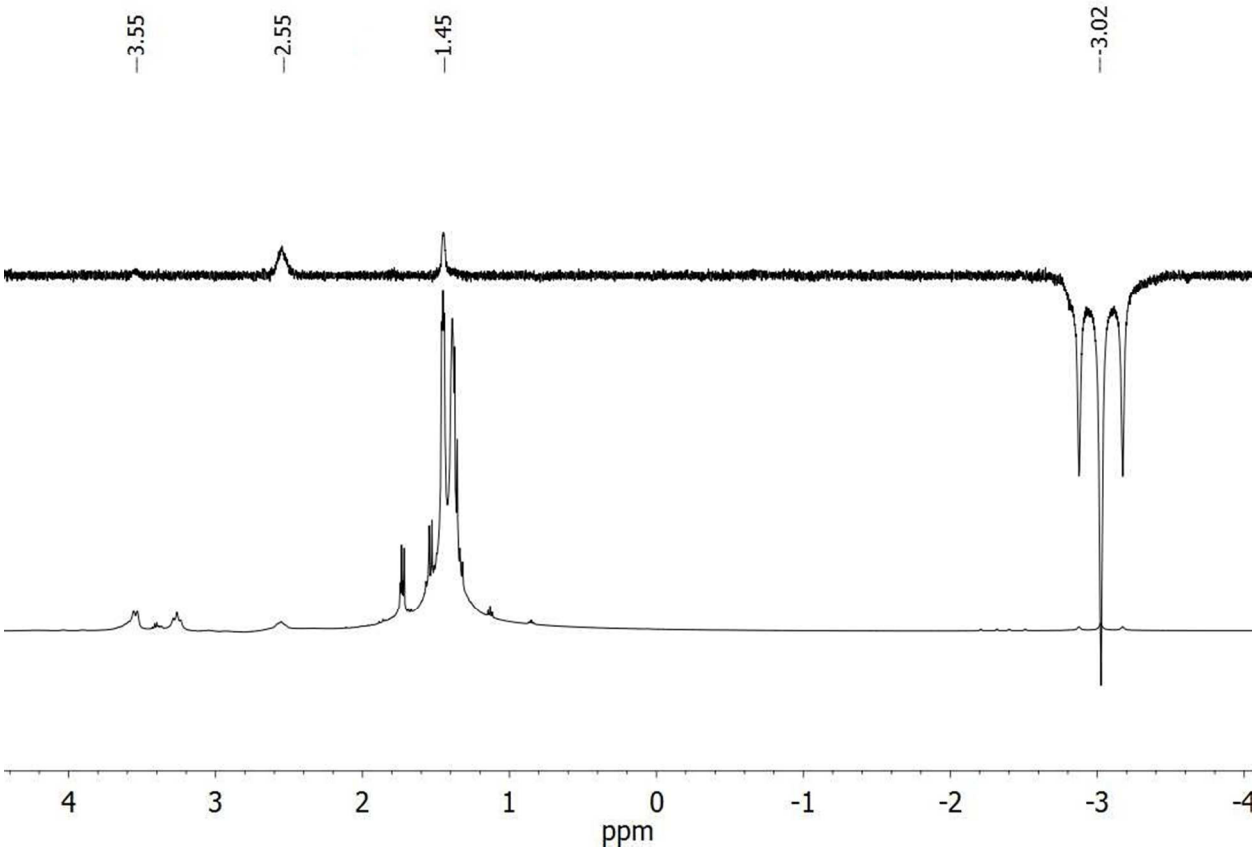

Figure S28. Rate of isomerization from [*t*-H**3'**]$^+$ to [μ-H**3**]$^+$ measured by monitoring the disappearance of terminal hydrides resonances from ^{1}H NMR spectrum in a CD_2Cl_2 solution at 20 °C.

Time dependence of concentration of [*t*-H**3'**]$^+$.

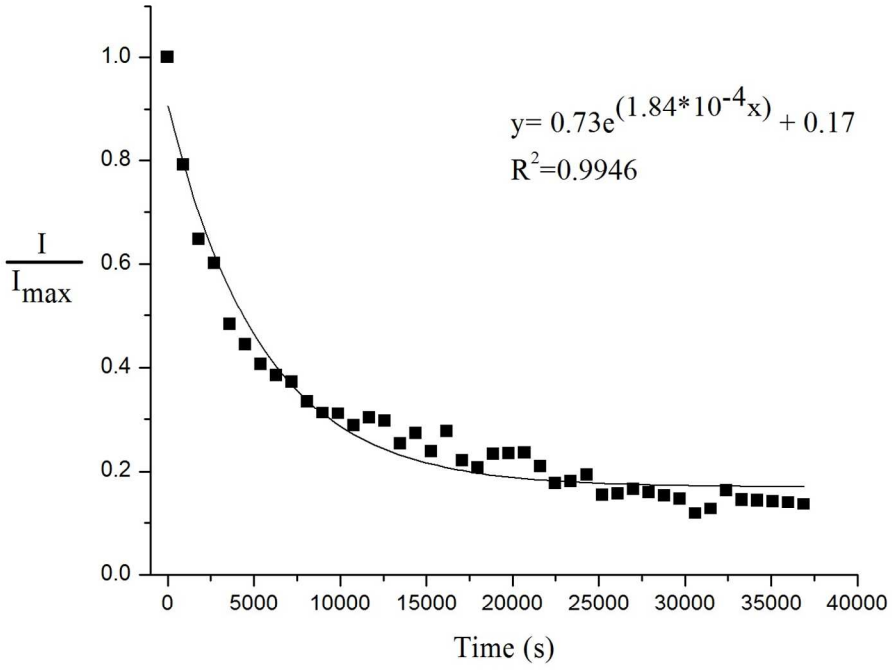

Time dependence of concentration of [μ-H**3**]$^{+}$.

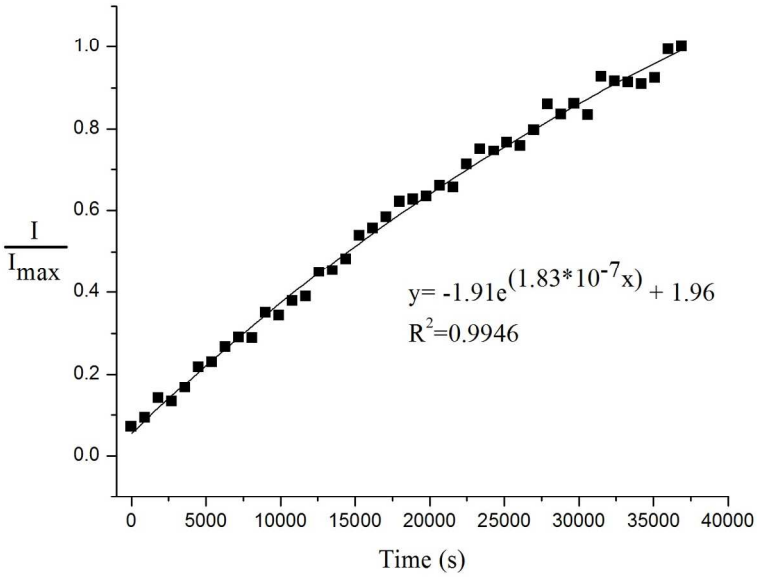

Time dependence of concentration of [*t*-H**3**]$^{+}$.

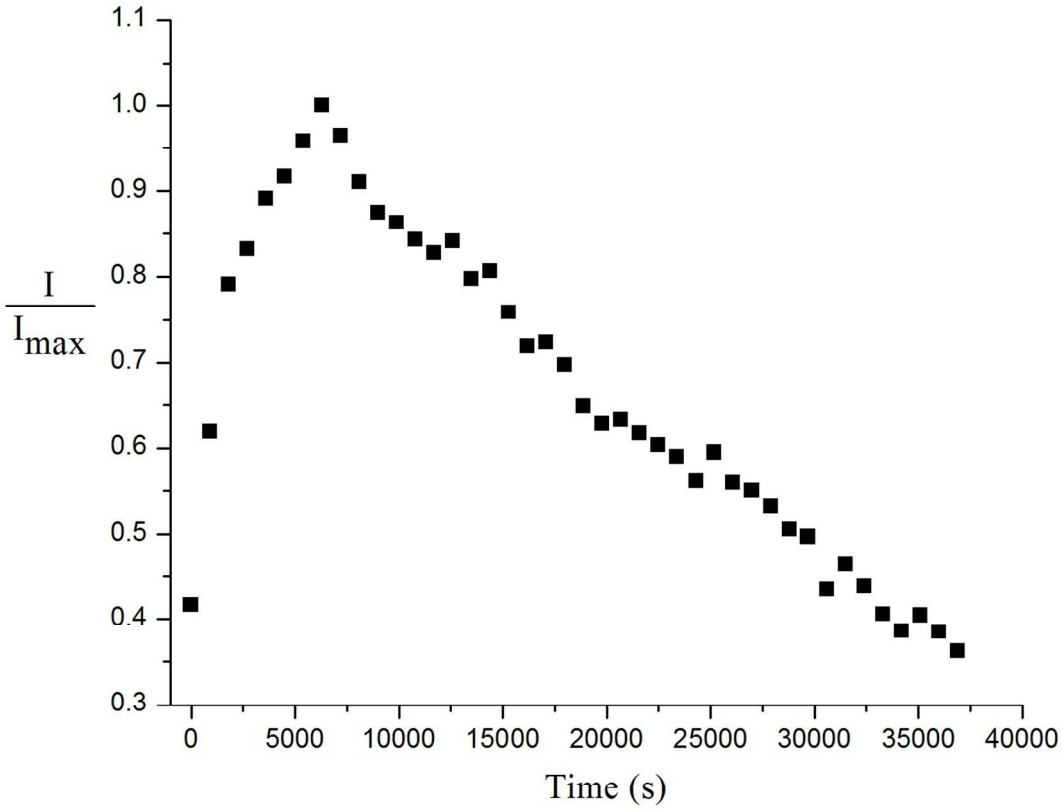

Composite of isomerization of [*t*-H**3**]$^+$.

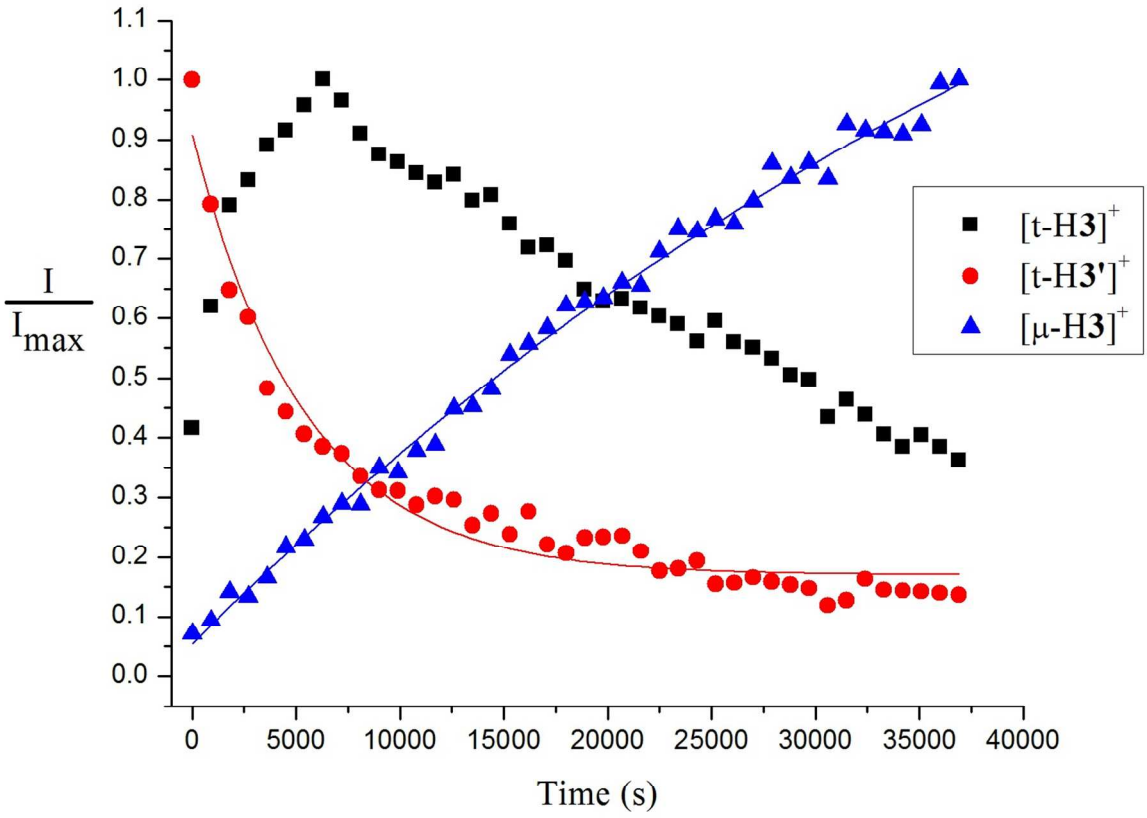

Figure S29. ^{1}H NMR spectrum of a CD_2Cl_2 solution of a mixture of the isomers of [*t*-$HFe_2(adtH)(CO)_2(PMe_3)_4](BF_4)(BAr^F{}_{20})$, [*t*-H**3**H]$(BF_4)(BAr^F{}_{20})$ and [*t*-H**3'**H]$(BF_4)(BAr^F{}_{20})$.

Assignment: The predominant isomer is [*t*-H**3**H]$^+$, which shows signals at δ –2.07 (dd, J_{PH} = 93.0, 55.4 Hz, 1H), 1.50 (d, J_{PH} = 11 Hz, PMe_3 9H), 1.53 (d, J_{PH} = 11 Hz, PMe_3 9H), 1.68 (d, J_{PH} = 11 Hz, PMe_3 9H), 1.80 (d, J_{PH} = 11 Hz, PMe_3 9H), 3.28 (t, C*H*HNH_2CH_2, 1H), 3.39 (t, CH_2NH_2CHH, 1H), 3.96 (m, CH*H*NH_2CH_2, 1H), 4.09 (m, CH_2NH_2CHH, 1H), 7.14 (broad s, $CH_2NH_2CH_2$, 1H), 8.13(broad s, $CH_2NH_2CH_2$, 1H). The other isomer is [*t*-H**3'**H]$^+$, which features an all-basal configuration of the phosphines. It shows signal for the terminal hydride δ –2.47 (t, J_{PH} = 73.4 Hz).

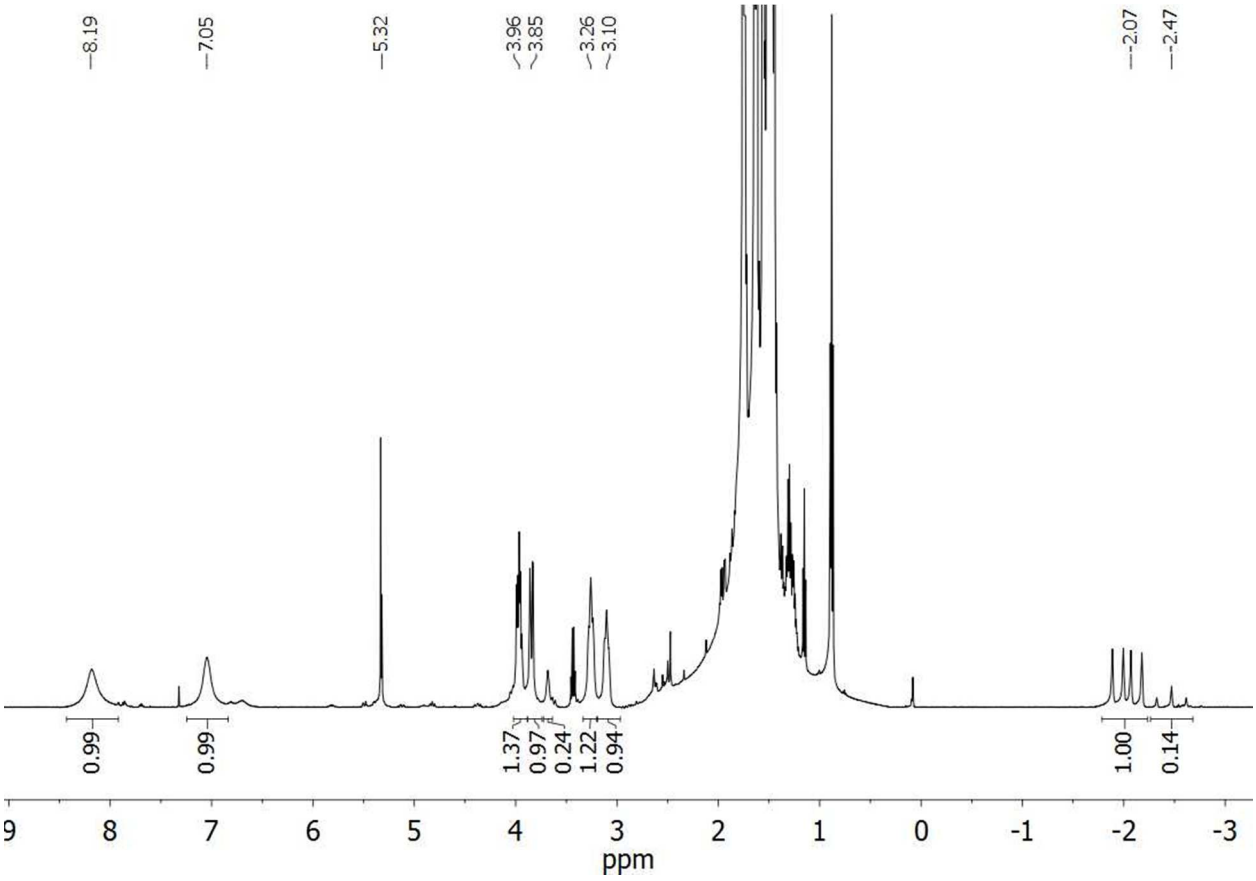

Figure S30. $^{31}P\{^{1}H\}$ NMR spectrum of a CD_2Cl_2 solution of a mixture of [*t*-$HFe_2(adtH)(CO)_2(PMe_3)_4](BF_4)(BAr^F{}_{20})$ isomers, [*t*-H**3**H][$(BF_4)(BAr^F{}_{20})$] and [*t*-H**3'**H][$(BF_4)(BAr^F{}_{20})$].

Assignments: The main isomer is [*t*-H**3**H]$^+$, which shows signals at δ 31.89 (d, J_{PH} = 42 Hz, 1P), 26,69 (d, J_{PH} = 42 Hz, 1P), 20.35 (d, J_{PH} = 42 Hz, 1P), 13.11 (d, J_{PH} = 42 Hz, 1P). The other isomer is [*t*-H**3'**H]$^+$, which features an all-basal configuration of the phosphines. It shows signals at δ 23.46 (s, 2P), 8.30 (s, 2P). The signal at δ -4.82 is for $HPMe_3^+$.

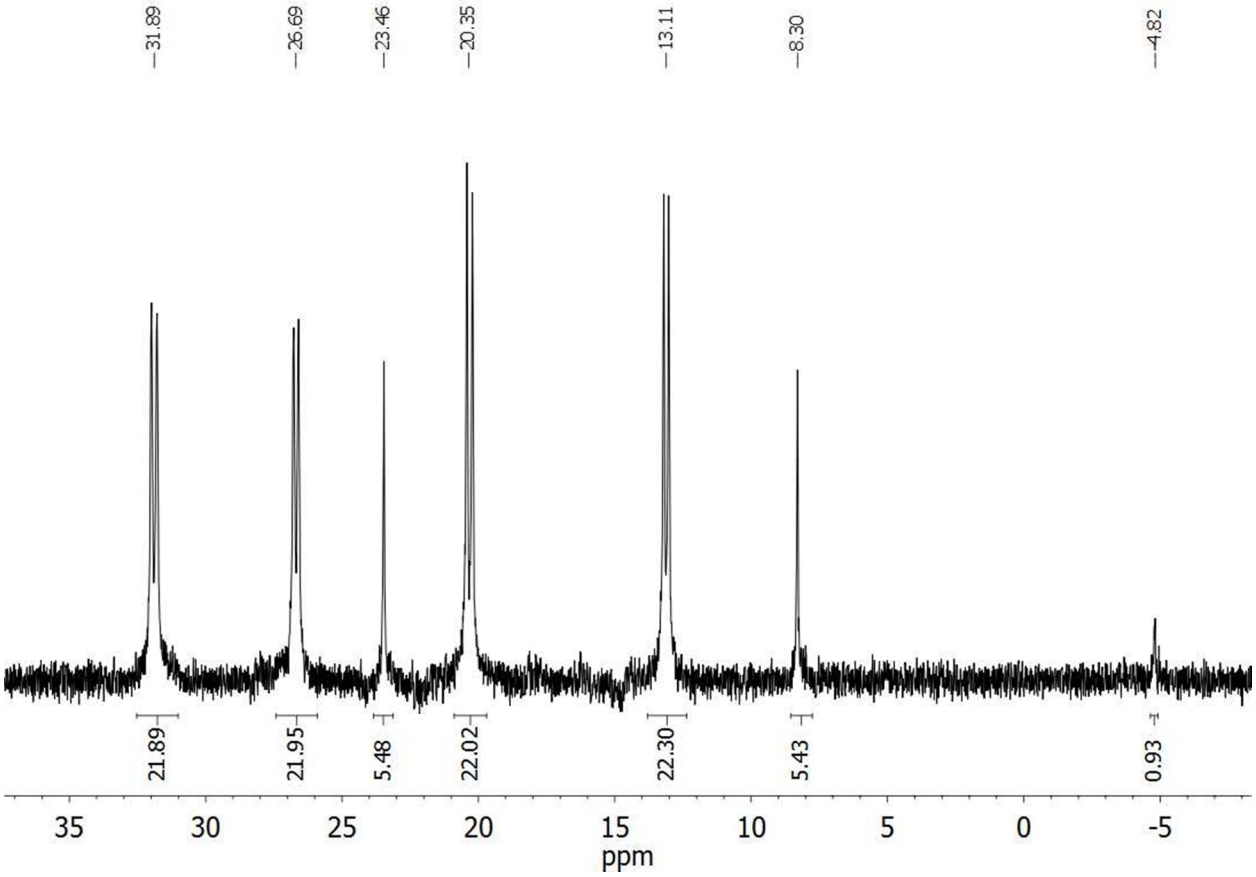

Figure S31. ^{1}H NMR spectrum (T = 20 °C) in the adt backbone region of a CD_2Cl_2 solution of [*t*-$HFe_2(adtH)(PMe_3)_4(CO)_2$]($BF_4$)($BAr^F_{20}$) before (top) and after (bottom) addition of one drop of D_2O. The signals on the bottom spectrum correspond to the amine-deuteride [*t*-D**3**]$^+$, indicating that water deprotonates the ammonium-hydride.

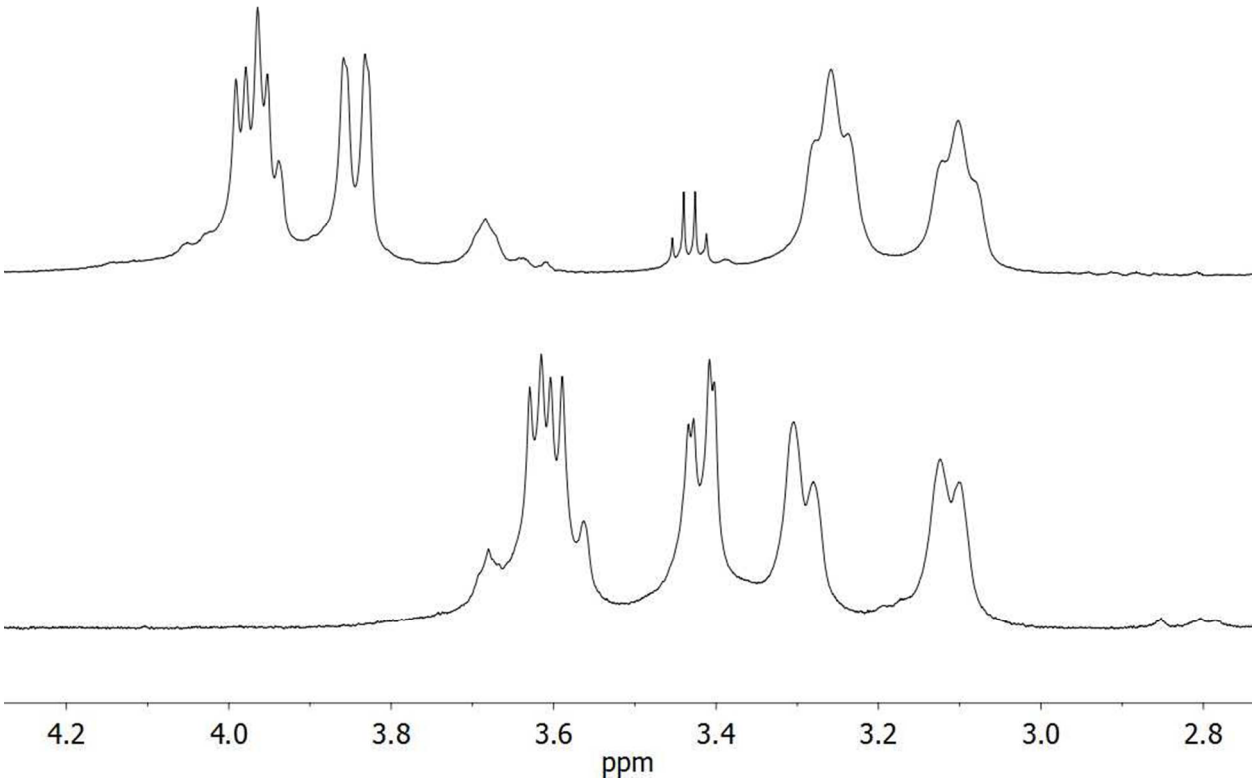

Figure S32. NOESY1D experiment on a CD_2Cl_2 solution of [*t*-H**3**H][(BF_4)(BAr^F_{20})] at -10 °C involving irradiation at δ -2.07.

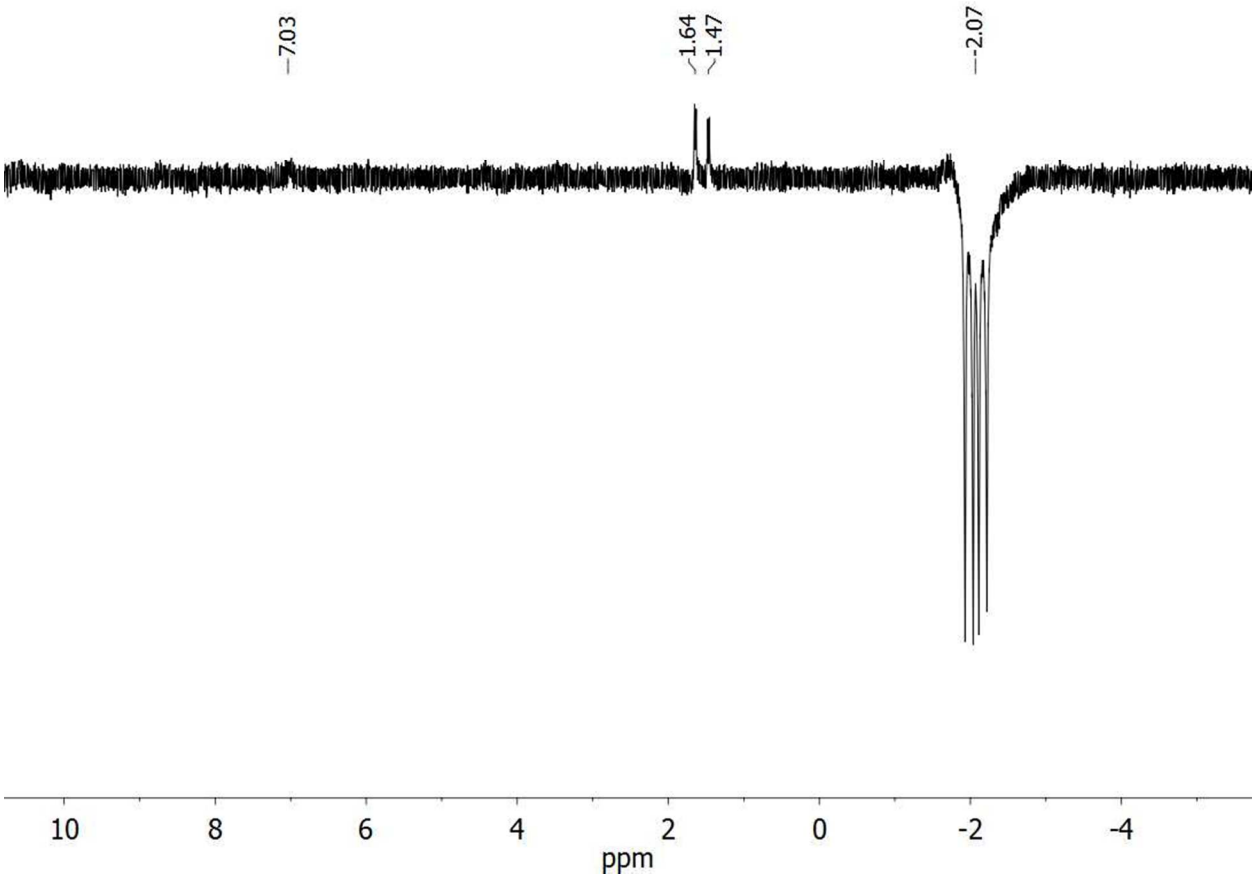

Crystallography of [*t*-H3]BAr$^F_4$ and [*t*-H3']BAr$^F_4$ (taken from .cif). The structure was phased by direct methods. Systematic conditions suggested the unambiguous space group. The space group choice was confirmed by successful convergence of the full-matrix least-squares refinement on F^2. The highest peaks in the final difference Fourier map were in the vicinity of the whole molecule disordered cation Fe, S and P atoms; the final map had no other significant features. A final analysis of variance between observed and calculated structure factors showed little dependence on amplitude or resolution.

Several data sets were collected on separate crystals. All data set exhibited the same whole cation disorder. Data were also collected with counter ion changed to pentafluorophenyl BAr$^F_4$. These crystals also showed whole cation disorder, although the packing was slightly different because the asymmetric unit also contained a molecule of Et_2O solvate. The final reported structure model was achieved using the data set that showed the highest bond precision with the best fitting parameters.

A structural model consisting of the whole cation disordered host plus a tetrakis(3,5-bis(trifluoromethyl)phenyl)borate counter ion ("BARF-24"). All of trifluoromethyl groups on the anion were highly disordered. The disorder was modeled with 3 sites, the sum of the three orientations being restrained to be unity and the primary, secondary and tertiary orientations of all 8 trifluoromethyl groups were restrained to be the same percent occupancies. All C-F bond distances and F-C-F bond angles were restrained to be similar (esd 0.03 and 0.05 Å, respectively). Similar displacement amplitudes (esd 0.01 Å) were imposed on F disordered sites overlapping by less than the sum of van der Waals radii, and their *U*'s were restrained to behave relatively isotropically (esd 0.01 Å). Once refined, the anion was constrained to behave as a rigid body in the final refinements to improve the data to parameter ratio.

Two isomers occupy the same location in the crystal. Disorder was deduced because atoms drifted to chemically unreasonable positions during the refinement. Many restraints were applied to force chemically similar bonding atoms to have similar bond distances and angles. The four PMe_3 groups in each isomer were restrained to have like C-P bond distances and like C-P-C angles (esd 0.02 and 0.04 Å, respectively). All Fe-P bond distances were restrained to be similar (esd 0.02 Å). Fe1-S1, Fe1-S2, Fe1b-S1b, Fe1b-S2b bond distances were also restrained to be similar (esd 0.02 Å). Like Fe1, Fe2-S positions were also restrained to be similar (esd 0.02 Å). The following bond pairs were individually restrained to be similar: Fe1-C1, Fe1b-C1b; C1-

O1, C1b-O1b; S2-C10, S1-C9, S2b-C10b, S1b-C9b; C10-N1, C9-N1, C10b-N1b, C9b-N1b (esd 0.02 Å). The hydride ligand was located in the difference map and then split between both cation orientations. Like Fe2-H bond distances were restrained to be similar (esd 0.01 Å). Additionally, to keep the hydrides from drifting to a chemically unreasonable location, the P3-H2, P4-H2, P3b-H2b, and P4b-H2b distances were restrained to be similar (esd 0.03 Å). The amine H atom was initially added geometrically as an aromatic N-H atom. The contraints were removed from the H atom and the N-H distances were fixed as 0.880(1) Å. To prevent the atom from drifting to a chemically unreasonable location, all like S(1/2)-H1(a/b) and C(9/10)-H1(a/b) distances were restrained to be similar (esd 0.01 Å). Rigid-bond restraints (esd 0.01 Å) were imposed on displacement parameters for all disordered cation sites and similar displacement amplitudes (esd 0.01 Å) were imposed on disordered sites overlapping by less than the sum of van der Waals radii. The displacement parameters for all P(CH$_3$)$_3$ atoms were also restrained to behave relatively isotropically. H atom treatment for the cations - methyl H atom positions were added geometrically with idealized C-H, R--H and H--H distances. Remaining H atoms were included as riding idealized contributors. Methyl H atom U's were assigned as 1.5 times Ueq of the carrier atom; remaining H atom U's, including the hydride H atoms, were assigned as 1.2 times carrier U_{eq}.

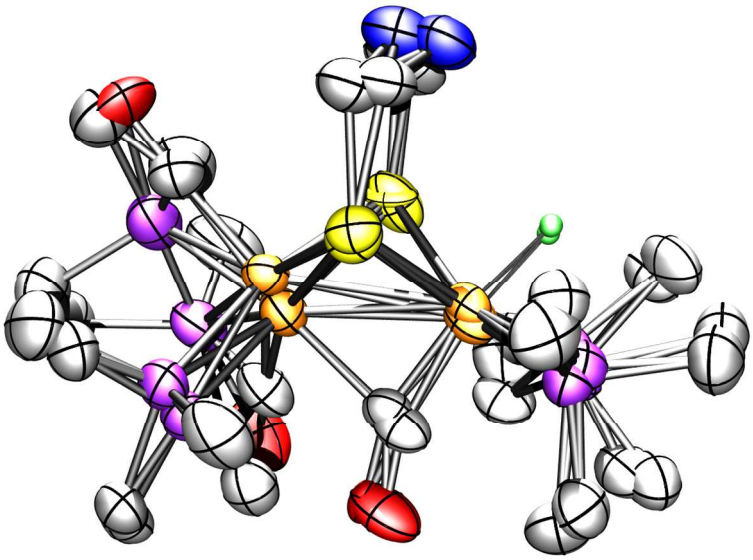

II. Supporting Information for DFT Calculations.

Figure SII-1. DFT-optimized structure of the lowest energy **1** isomer. Distances in Å.

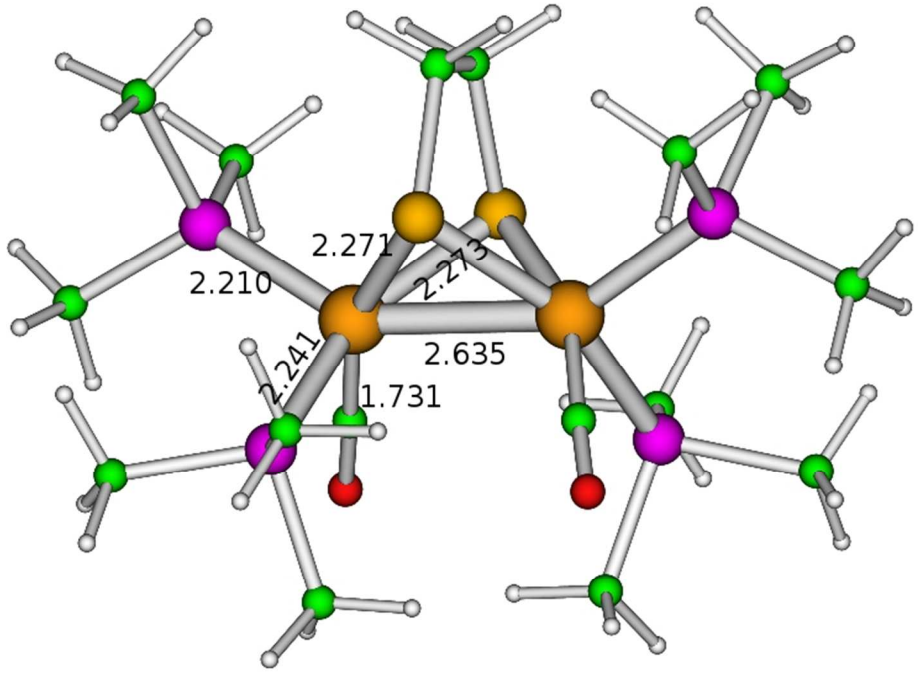

Figure SII-2. DFT-optimized structures of the lowest energy **2** isomers. Distances in Å.

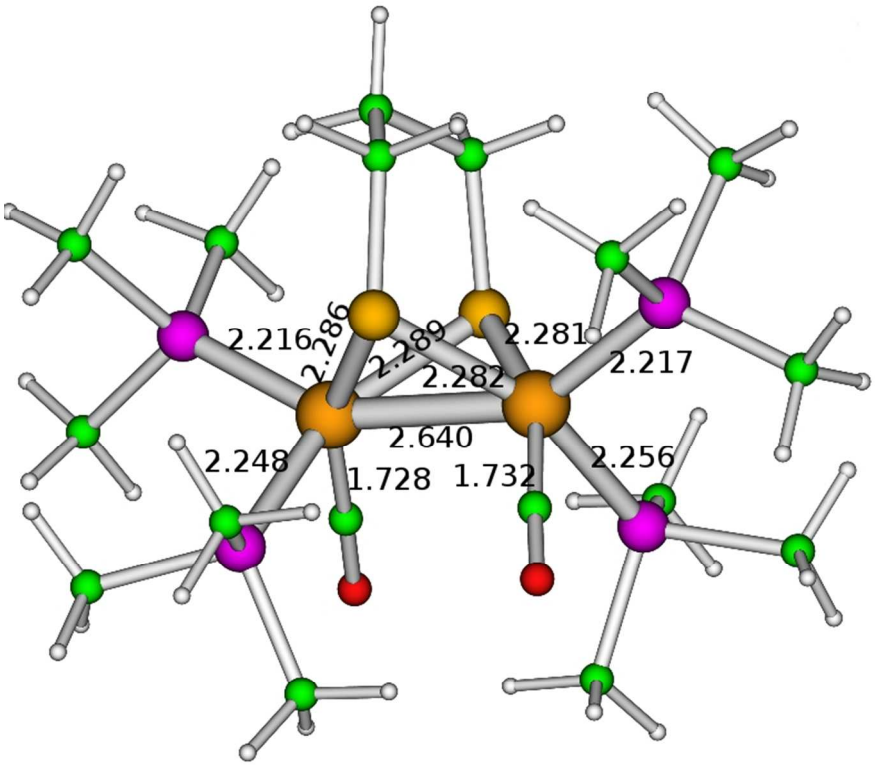

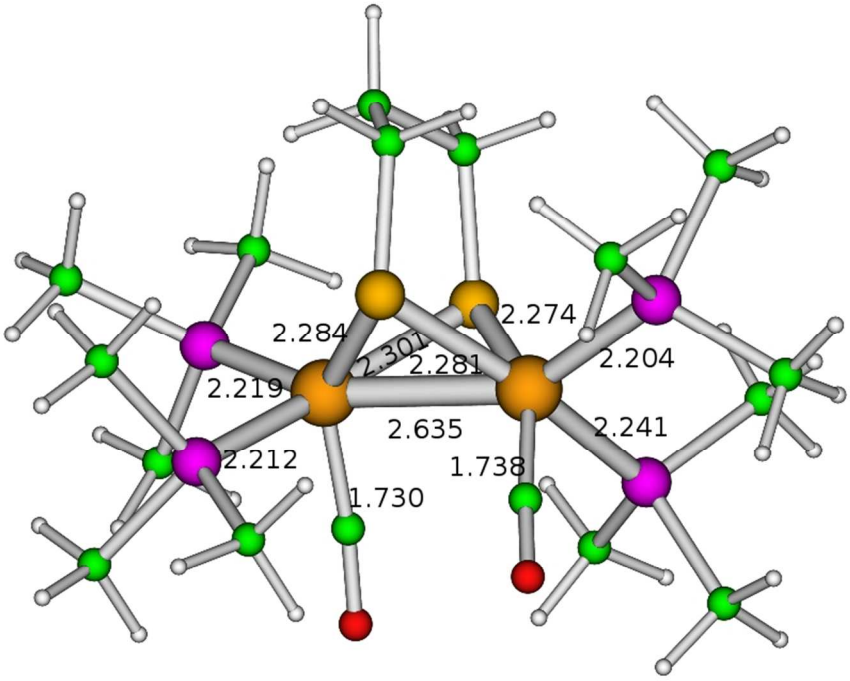

Scheme SII-3. Computed relative stability of protonated derivatives of **2** (energies in kcal/mol). Very similar results (within 2 kcal/mol) were obtained for **1** (data not shown).